SANDIA REPORT
SAND2015-10092
Unlimited Release
Printed November, 2015

Design, Construction, and Operation of a Supercritical Carbon Dioxide (sCO_2) Loop for Investigation of Dry Cooling and Natural Circulation Potential for Use in Advanced Small Modular Reactors Utilizing sCO_2 Power Conversion Cycles

Bobby D. Middleton, Salvador Rodriguez, Matthew Carlson

Prepared by
Sandia National Laboratories
Albuquerque, New Mexico 87185 and Livermore, California 94550

Sandia National Laboratories is a multi-program laboratory managed and operated by Sandia Corporation, a wholly owned subsidiary of Lockheed Martin Corporation, for the U.S. Department of Energy's National Nuclear Security Administration under contract DE-AC04-94AL85000.

Issued by Sandia National Laboratories, operated for the United States Department of Energy by Sandia Corporation.

Available to DOE and DOE contractors from
U.S. Department of Energy
Office of Scientific and Technical Information
P.O. Box 62
Oak Ridge, TN 37831

Telephone: (865) 576-8401
Facsimile: (865) 576-5728
E-Mail: reports@adonis.osti.gov
Online ordering: http://www.osti.gov/bridge

Available to the public from
U.S. Department of Commerce
National Technical Information Service
5285 Port Royal Rd.
Springfield, VA 22161

Telephone: (800) 553-6847
Facsimile: (703) 605-6900
E-Mail: orders@ntis.fedworld.gov
Online order: http://www.ntis.gov/help/ordermethods.asp?loc=7-4-0#online

SAND2015-10092
Unlimited Release
Printed November 2015

Design, Construction, and Operation of a Supercritical Carbon Dioxide (sCO_2) Loop for Investigation of Dry Cooling and Natural Circulation Potential for Use in Advanced Small Modular Reactors Utilizing sCO_2 Power Conversion Cycles

Bobby D. Middleton†, Salvador Rodriguez, and Matthew Carlson
Advanced Nuclear Concepts Department
Sandia National Laboratories
P.O. Box 5800
Albuquerque, New Mexico 87185-MS1136

† Point of Contact Author

Abstract

This report outlines the work completed for a Laboratory Directed Research and Development project at Sandia National Laboratories from October 2012 through September 2015. An experimental supercritical carbon dioxide (sCO_2) loop was designed, built, and operated. The experimental work demonstrated that sCO_2 can be utilized as the working fluid in an air-cooled, natural circulation configuration to transfer heat from a source to the ultimate heat sink, which is the surrounding ambient environment in most cases. The loop was also operated in an induction-heated, water-cooled configuration that allows for measurements of physical parameters that are difficult to isolate in the air-cooled configuration. Analysis included the development of two computational fluid dynamics models. Future work is anticipated to answer questions that were not covered in this project.

This page intentionally left blank.

Contents

FIGURES

TABLES

NOMENCLATURE

APS	Arizona Public Service
aSMR	Advanced Small Modular Reactor
BC	Boundary Condition
CFD	Computational Fluid Dynamics
DOE	Department of Energy
EIA	Energy Information Administration
EPEC	El Paso Electric Company
Gr	Grashof number
GWe	Gigawatts Electric
HS	Heat Structure
kPa	Kilopascal
LADWP	Los Angeles Department of Water and Power
LDRD	Laboratory Directed Research and Development
LES	Large Eddy Simulation
LWR	Light Water Reactor
MPa	Megapascal
MWe	Megawatts Electric
ORNL	Oak Ridge National Laboratory
PNM	PNM Resources (Public Service Company of New Mexico Resources)
PVNGS	Palo Verde Nuclear Generating Station
PWR	Pressurized Water Reactor
RTD	Resistance Temperature Detector
sCO_2	Supercritical Carbon Dioxide
SCE	Southern California Edison
SCPPA	Southern California Public Power Authority
SMR	Small Modular Reactor
SNL	Sandia National Laboratories
SRP	Salt River Project
TAC	Turbine-alternator-compressor
TC	Thermocouple
US	The United States of America

1 INTRODUCTION

Small modular nuclear reactors (SMRs) have recently received a great deal of attention. Generally, SMRs are separated into two categories: light water reactor-cooled (LWR) SMRs and SMRs that are designed to use a coolant other than light water. Another distinction among the various SMR designs can be made when considering the power conversion technology that is utilized. Currently, most operating nuclear power plants utilize a traditional steam Rankine power conversion cycle. However, recent advances in engineering have made alternate power conversion cycles – most notably Brayton cycles – more feasible. For the purpose of this report, any SMR that utilizes a primary coolant other than light water, or utilizes any power conversion cycle other than a steam Rankine cycle, will be considered an advanced SMR (aSMR).

Sandia National Laboratories (SNL) is a recognized leader in supercritical carbon dioxide (sCO_2) Brayton cycle technologies. Therefore, extending this expertise into the realm of dry heat rejection and natural circulation by utilizing sCO2 is a natural process for SNL. In 2012, SNL commissioned an internal experimental project on the use of sCO_2 as a potential working fluid for natural circulation and dry heat rejection for aSMRs that utilize a sCO_2 Brayton cycle for power conversion. This project involved the design and construction of an experimental loop that would exhibit the ability of sCO_2 to provide circulation with no pumps while utilizing air for heat rejection.

1.1 Background

In the United States (US), most operating nuclear power plants (excluding research reactors) are large-capacity LWRs. As of July, 2015, the Department of Energy's (DOE) Energy Information Administration (EIA) lists 99 operating commercial nuclear power plants in the US, with a total power rating of 103.86 gigawatts-electric (GWe). This gives an average of about 1049 megawatts-electric (MWe) per reactor. The smallest of these reactors is the reactor at Fort Calhoun Nuclear Generating Station, with a rating of 502 MWe. The largest is the reactor at Grand Gulf Nuclear Generating Station, with a rating of 1440 MWe [1]. There are also five nuclear reactors currently under construction in the US. All of them are pressurized water reactors (PWRs). Four of them (two at Vogtle Electric Generating Plant and two at Virgil C. Summer Nuclear Generating Station) are rated at 1200 MWe each and the other (Watts Bar 2) is rated at 1218 MWe [2].

The major driving force behind the interest in SMRs is economic. Estimates suggest construction of a new LWR of traditional design would represent an investment on the order of $10 Billion. It is difficult for most utilities to accept incurring this level of financial risk since the failure of such a venture could potentially spell the end of that utility. Therefore, the prospect of a lower capital cost is appealing to a utility interested in nuclear power, even if the cost per unit of energy produced projects to be higher than that of a large, traditional nuclear power plant [3]. This economic driving force has led to a large amount of interest in SMRs in recent years.

Sandia National Laboratories has been a leader in Brayton cycle research since the early 2000s. In 2007, SNL began funding an internal Laboratory Directed Research and Development (LDRD) project to build and operate a sCO_2 compressor research loop to investigate compressor operation and control just above the critical point of CO_2. The goal of this work was to understand the engineering and operational requirements of using sCO_2 as the working fluid in a power conversion cycle. The focus on operation and

control around the critical point was due to the extreme property changes that occur near the critical point; these property changes have both a positive effect and a negative effect when a sCO_2 Brayton cycle is being considered for power conversion. Near the critical point, CO_2 has a density that is more than half that of water. This allows for a very high compressor efficiency, much closer to that of a pump than what is generally considered for a compressor. However, the density – as well as other thermodynamic properties, such as specific heat capacity – of CO_2 can also change drastically with a very small change in temperature. The drastic changes in fluid properties can potentially lead to concerns related to system stability, including some issues with thrust bearing longevity in the turbine-alternator-compressor (TAC) unit [4]. Figure 1is a plot of the constant-pressure specific heat (C) capacity near the critical point, plotted on a logarithmic scale. As can be seen, C_p begins changing drastically near the critical temperature (304.1 K). It is sometimes more informative to plot the inverse of this data near the critical point since C_p diverges at the critical point. Figure 2is a plot of inverse specific heat capacity as a function of both temperature and pressure near the critical point (304.1 K, 7.38 MPa). The ridge in this plot traces the values of C_p at the pseudocritical points and the spikes along this ridge are due to a numerical artifact in the REFPROP database [5]. The discontinuity at the center of Figure 2 marks the critical point. The data at lower pressures are from the two-phase region of CO_2, while the data at higher pressures are from the supercritical region.

While sCO_2 Brayton cycle work has been ongoing at SNL and elsewhere, little attention has been paid to some of the other benefits of sCO_2 properties until 2012. In 2012, SNL began funding a LDRD project to investigate two different cases whereby CO_2 would be beneficial for aSMRs. The two cases are:

1. Dry heat rejection of an aSMR using a sCO_2 Brayton cycle for power conversion and
2. Use of sCO_2 in a naturally circulating decay heat removal system for an aSMR.

The project was funded to investigate the properties of sCO_2 near the critical point and to demonstrate the feasibility of using sCO_2 as the working fluid in either of the aforementioned cases. The general process involved:

1. Design of the loop,
2. Procurement of equipment,
3. Construction of loop,
4. Shakedown testing of loop,
5. Design of experiments,
6. Operation of loop,
7. Analysis of data, and
8. Reporting of results.

This report outlines these steps and concludes the LDRD project.

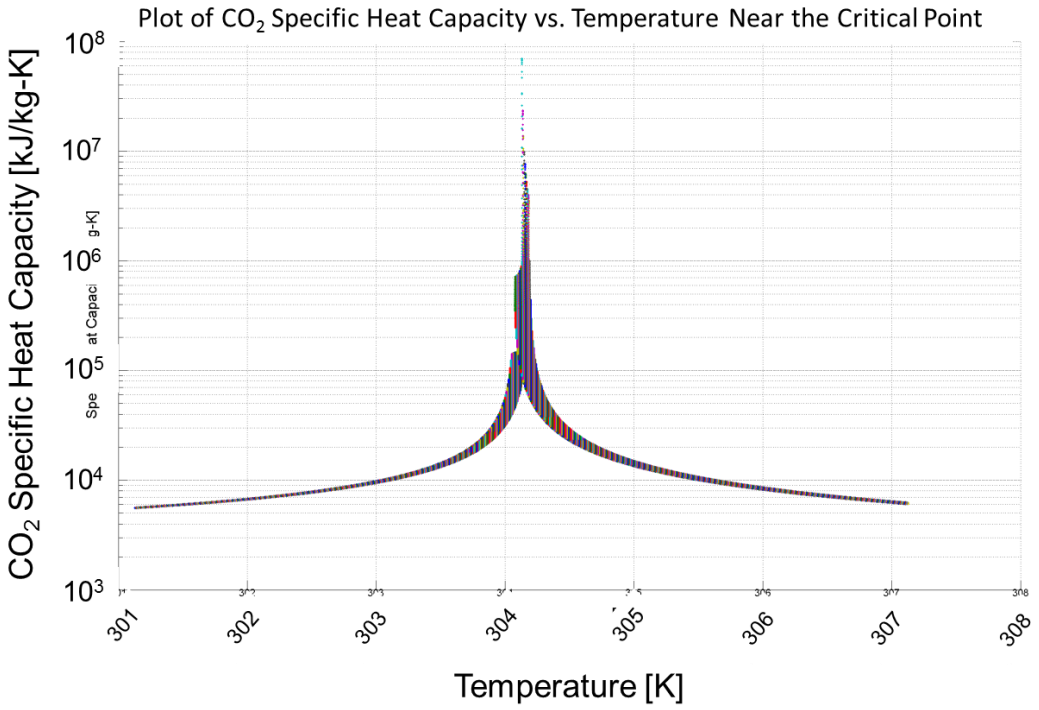

Figure 1 Plot of CO_2 specific heat capacity as a function of temperature near the critical point. The data was taken from REFPROP version 9.1 [5].

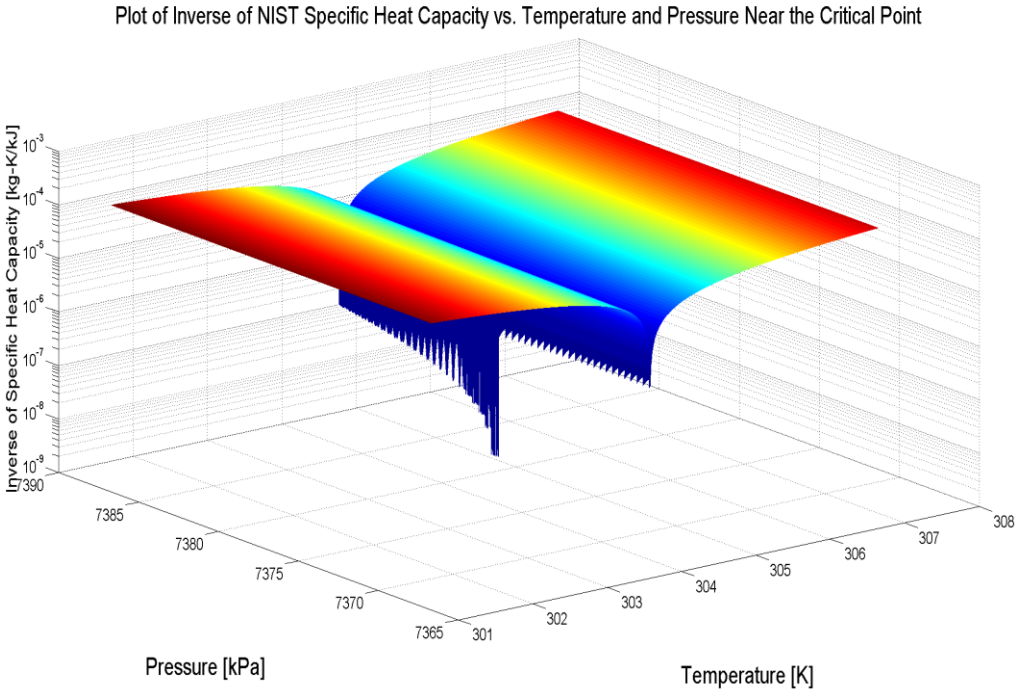

Figure 2 Plot of inverse of CO_2 specific heat capacity as a function of temperature and pressure near the critical point. The data was taken from REFPROP version 9.1 [5].

1.2 Scope

1.2.1 SCO2 as an Enabling Fluid for Dry Heat Rejection

SMRs continue to be proposed as a means of meeting ever-increasing energy needs throughout the world, both for electricity production and for thermal energy production. The currently available designs are all LWRs. These designs all use traditional steam Rankine cycles for power production.

It is likely that the next generation of SMRs will be comprised of breeder reactors. Breeder reactors can help create a nuclear fuel cycle that allows the extraction of nearly 100% of the energy in natural uranium, as opposed to the less than 1% that is extracted in current once-through LWR cycles. These reactors all offer the promise of a high power density in comparison with LWRs and they purport to operate at much higher temperatures than current LWR technology. The high-temperature heat can be useful for multiple process applications. The high operating temperature also increases the efficiency of the power conversion cycle, the most common of which is currently a steam Rankine cycle. Breeder reactors use a fast neutron spectrum. Since water is a very effective moderator for neutrons, water would most likely not be used as a coolant in a well-designed breeder reactor. Some likely coolants for these reactors are: high-temperature gas, some form of liquid metal, or some form of molten salt.

Higher operating temperatures could allow aSMRs to be coupled with a high-temperature Brayton cycle for power conversion. This could mark a significant advance in the efficiency, sizing, and economics of nuclear power. A secondary benefit is the ability to utilize air instead of water for ultimate heat rejection. Water is becoming more and more difficult to obtain for power production purposes, and consequently, more expensive. Thermoelectric power generation is the single largest user of water withdrawals in the US; in 2011, this equated to about 196 billion gallons of water per day (~71.5 trillion gallons per year) and represented about 48.5% of all water withdrawals in the US. Most of this water (~70.4%) is fresh surface water being withdrawn [6]. Figure 3 is a flow chart of energy and water in the US.

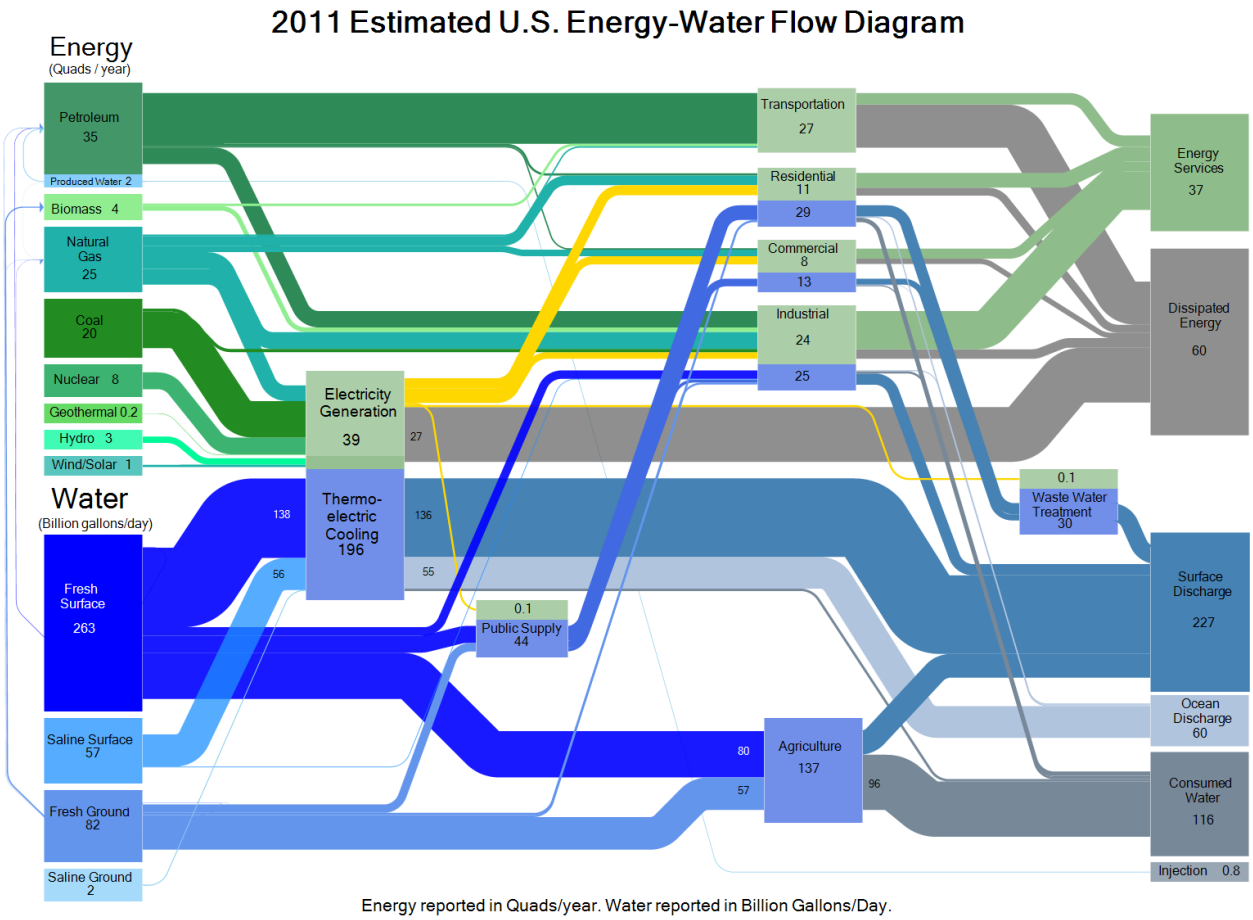

Figure 3 Estimated US energy and water flow for 2011. Taken from Bauer, 2014 [6].

Nuclear power is dependent upon water availability, due to its use in moderating and cooling nuclear reactors. A recent study by the Oak Ridge National Laboratory (ORNL) assessed the siting potential for nuclear power plants throughout the continental US. One of the major contributing factors was the availability of water for cooling (**Error! Reference source not found.**) [7]. As can be seen in the figure, most of the western portion of the US is excluded from new nuclear power generation; much of this is due to a lack of water.

One example of this price increase of water can be seen at the Palo Verde Nuclear Generating Station (PVNGS). PVNGS is owned by multiple entities, including the Arizona Public Service (APS), the Salt River Project (SRP), the El Paso Electric Company (EPEC), Southern California Edison (SCE), PNM Resources (PNM), the Southern California Public Power Authority (SCPPA), and the Los Angeles Department of Water and Power (LADWP). PVNGS is located west of Phoenix, Arizona. It is the only nuclear generating station in the world that is not located near a large body of water. It instead relies on reclaimed water from local townships for evaporative cooling of the plant. In 2010, PVNGS renewed an agreement to purchase water from five cities around the station, but the cost increased sharply from the previous purchase agreement. Under the current agreement, the cost of water will increase at a rate of 10.5% per year until 2025. From 2026 until 2050, the rates will still increase but will be based on a tiered

formula, with the cost per unit of water increasing as water usage increases [8]. The contract ends in 2050.

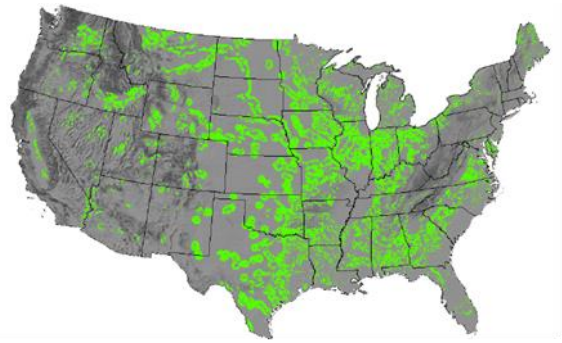

Green: areas of sufficient water

[Mays, 2012]

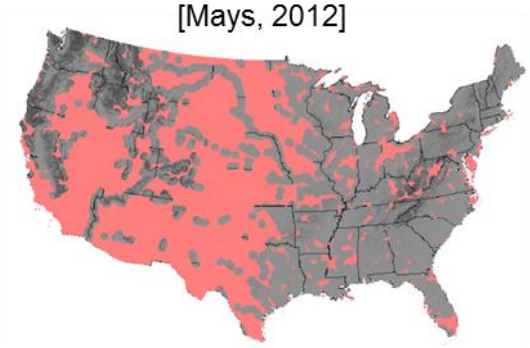

Pink: areas excluded from nuclear siting

Figure 4 Illustration of areas in continental US where siting of nuclear power is possible. The green areas have sufficient water, while the pink areas are excluded from nuclear siting [7].

Power generation cooling is almost entirely encompassed by four general types of cooling arrangements (**Error! Reference source not found.**) [10]. They are:

1. Once-through Cooling – Water is withdrawn from a river, lake, or other natural water source, pumped through a condenser to cool/condense the steam exiting the turbine of a power conversion cycle, then returned to the natural water source. Little to no evaporation takes place. However, the discharged water has a higher temperature than the withdrawn water, thus contributing to some environmental effect.

2. Wet Cooling Tower – Wet cooling towers can be divided into two sub-categories:
   a. Direct (Open Circuit) Wet Cooling – The water being used to cool the working fluid of the power conversion unit is passed through a cooling tower, making direct contact with the air being used to evaporate the cooling water. The water that is lost to evaporation is replaced with "makeup" water from the natural water source.
   b. Indirect (Closed Circuit) Wet Cooling – The water being used to cool the working fluid of the power conversion unit is in a closed circuit and never makes direct contact with the air. Instead, water from the natural water source is passed over the outside of the piping

that is used to recirculate the cooling water. Air is also made to pass over the freshwater supply, causing it to evaporate, thereby "indirectly" cooling the plant.

3. Dry Cooling Tower – The water being used to cool the working fluid of the power conversion unit is routed to a header, which then directs the hot fluid into a specially-designed water-to-air heat exchanger. Either forced or natural draft air is used to cool the water, which is recirculated to the plant. This type of cooling does not evaporate water, but it does decrease power conversion efficiency.

4. Hybrid Cooling Tower – A hybrid cooling tower combines both the wet and dry cooling tower concepts into one device. Typically, the portion of steam that is passed through the dry cooling circuit decreases as the ambient temperature increases. In this way, an optimum strategy can be developed that will minimize losses due to the decreased efficiency caused by dry cooling.

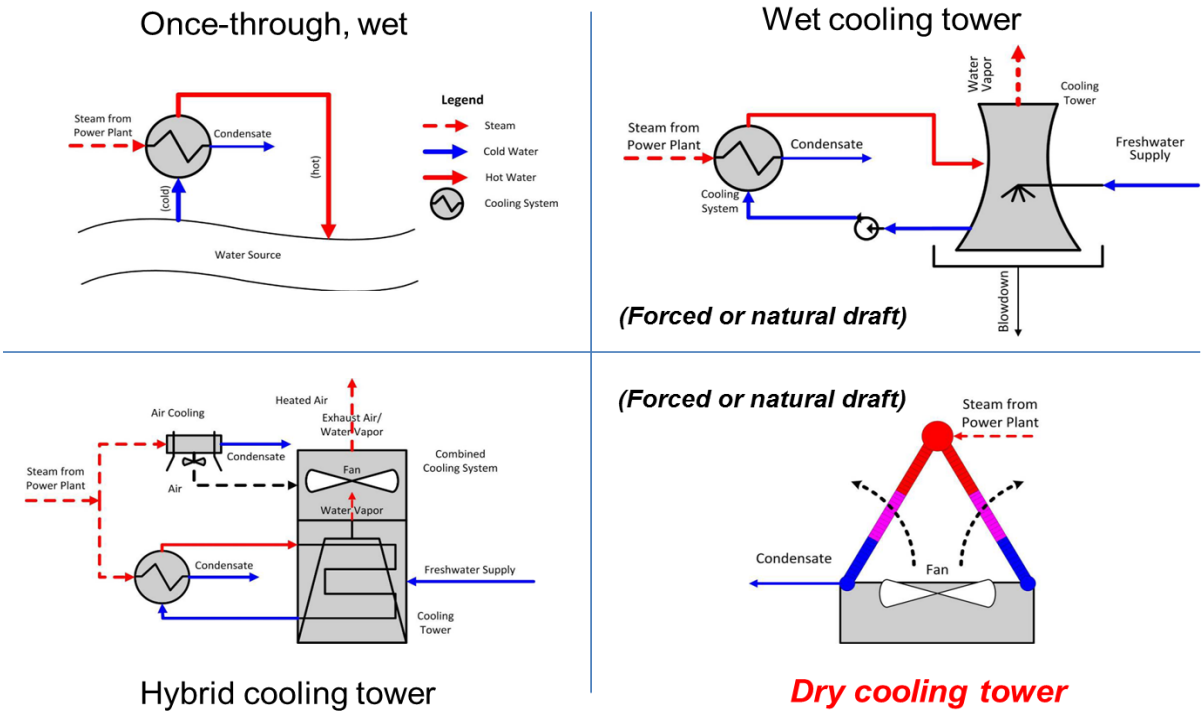

Figure 5 Illustration of four basic types of cooling options for large-scale power generation [10].

SCO_2 Brayton cycles offer the potential to greatly reduce the amount of water needed for thermoelectric power production. Although work has been ongoing in the area of dry heat rejection, much of it has focused on ultimate heat rejection for steam cycles. Dry heat rejection of a steam cycle implies that the temperature difference between the steam and the air into which the heat is transferred will decrease as the air passes through the heat exchanger. This concept is illustrated in **Error! Reference source not found.** [10]. As heat transfer is proportional to the temperature difference in the two fluid streams, this

decrease in temperature difference represents a fundamental physical limit to the efficiency of dry heat rejection from steam power conversion cycles. Most ongoing research focuses on improving heat exchanger surface effects and on new heat exchanger materials.

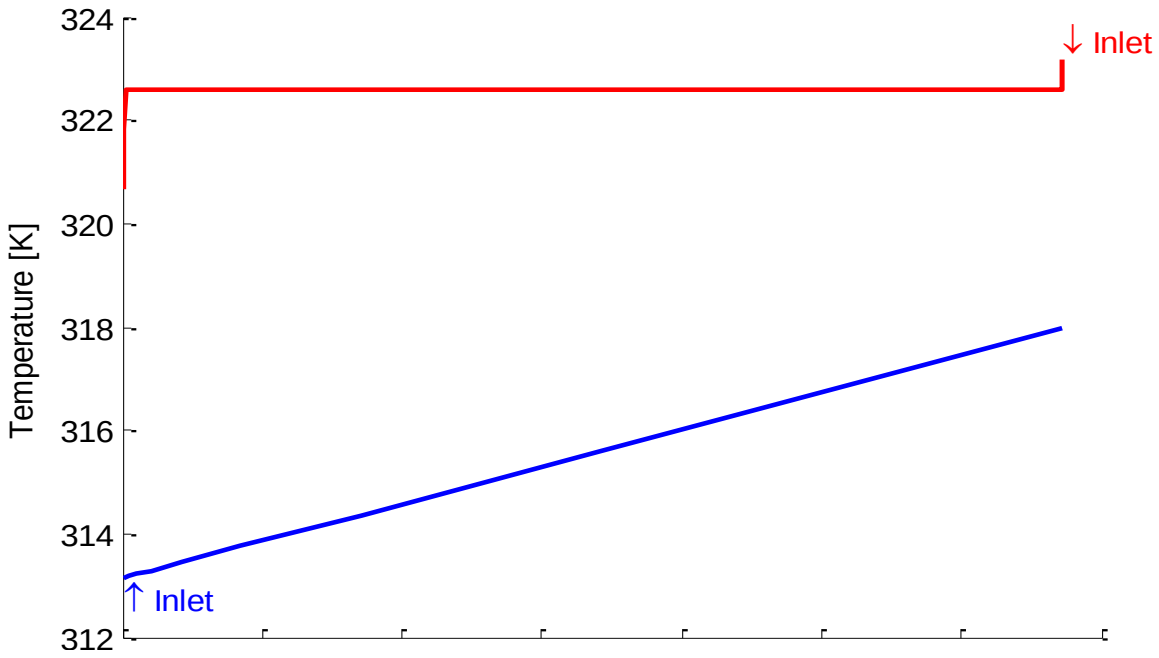

Figure 6 Illustration of decreasing temperature difference between cooling air and steam for a dry-cooled steam cycle [10].

Prior to the current LDRD project, the use of an alternative working fluid has been relatively unexplored [11]. A sCO_2 Brayton cycle does not have the same temperature difference limitation that is inherent in a steam Rankine cycle. Since the working fluid of a sCO_2 Brayton cycle is a single-phase fluid above the critical point, it is feasible that the temperature difference between the heat source and the heat sink can be made to be nearly constant throughout the heat transfer region. This concept is illustrated in **Error! Reference source not found.** [10]. The comparisons made in this figure are based on ambient air temperature of 40° C, exit temperature of the working fluid of 50° C, a minimum temperature difference (pinch) of 5° C, and a heat exchanger duty of 20 kW for both types of power conversion cycle. With these assumptions, the air flow required to cool a steam Rankine power conversion cycle is 17 times that required to cool a sCO_2 power conversion cycle. In practice, the operating pressure of the steam cycle would most likely be raised from 13.0 kPa to 16.5 kPa, thereby raising the temperature of the steam and decreasing both the air flow required and the efficiency of the power conversion cycle. Even in this case, the air flow required for the steam cycle would be about six times that required for the Brayton cycle.

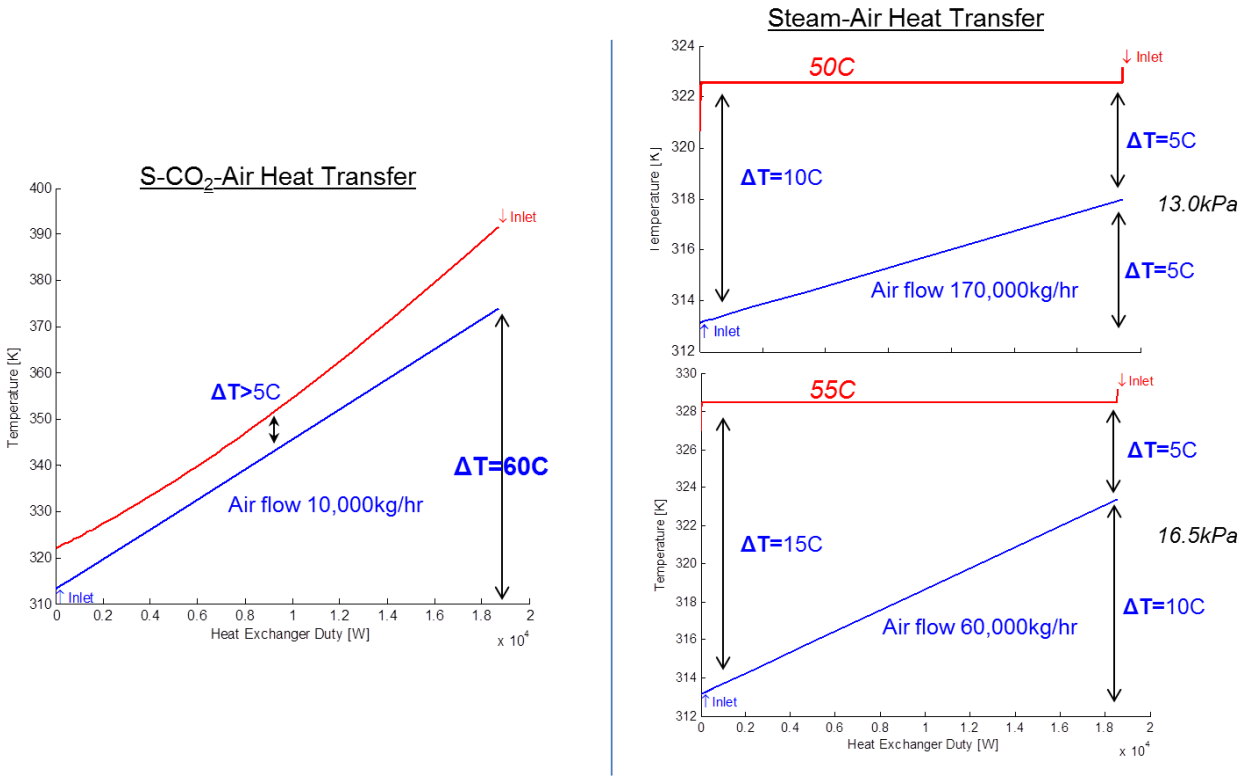

Figure 7 Comparison of air flow rate required for sCO2 Brayton and steam Rankine cycles [10].

It is possible that the cost of air cooling can be decreased to the point that it is comparable to that of water cooling by incorporating sCO_2 Brayton technology couple with dry heat rejection. If so, this improvement in technology could have a positive effect on the availability of electricity, especially in arid regions throughout the world.

Recent studies have suggested that dry cooling of a sCO_2 power conversion cycle can be comparable to that of wet cooling for a steam turbine cycle. **Error! Reference source not found.** illustrates the estimated number of cooling towers required for a 1333 MWe sCO_2 cooling plant with dry cooling towers (50° C ambient air temperature), a 1000 MWe steam turbine plant with dry cooling towers (55° C ambient air temperature), and a 1100 MWe steam turbine plant with wet cooling towers (35° C cooling water temperature). As can be seen, the number of cooling towers needed for the sCO_2 Brayton cycle is dramatically fewer than that needed for the steam turbine plant with dry cooling. It is, in fact, fewer than the number of wet cooling towers needed for a steam turbine plant [11].

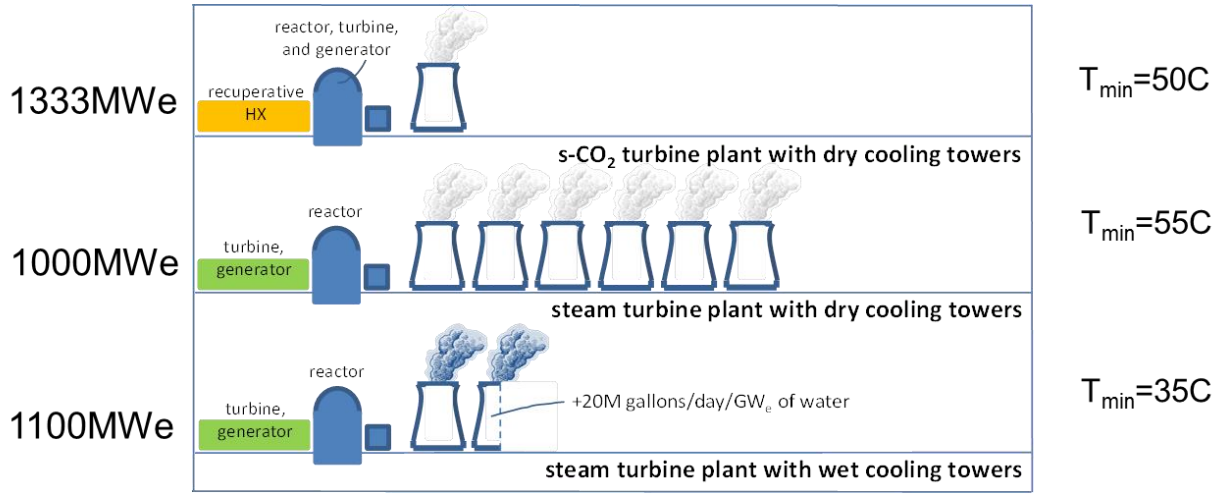

Figure 8 Comparison of number of cooling towers needed for various power conversion cycles [11].

Adoption of dry cooling towers has been almost nonexistent. As of 2013, only about 1% of power generating capacity was cooled with dry cooling. This is due mainly to economic reasons. Dry cooling towers are estimated to be 3-5 times as expensive to build as closed-cycle wet cooling towers and can be 10 times as expensive to operate. The operational costs can come from a gross decrease in plant efficiency plus the indirect cost of operating the cooling fans if force air is employed. Table 1 presents some statistics on the use of different cooling configurations and on the relative costs and water usage [12]. In general, about 90% of all water used at power plants is used for cooling. The other 10% is used for cleaning, makeup water, and personal use, etc. [13]. As can be seen from the data in Table 1, if dry cooling could be implemented in even a small fraction of power generating facilities, it could reduce water usage by more than a 100% reduction in makeup water and other uses at power plants. This alone could make sCO_2 Brayton cycles and their associated dry cooling benefits worth the investment in time and other resources to bring them to market.

Table 1 Relative use of different cooling technologies and their impacts on water flow [12].

Cooling System	Percent of Generating Capacity Using this Technology	Cost Ratio Relative to Wet Cooling Tower	Evaporative Loss Ratio Relative to Wet Cooling Tower	Coolant Flow Ratio Relative to Wet Cooling Tower
Once-Through Cooling	43%	0.4-0.75	~0.4	~1.25
Closed-Cycle Wet Cooling	42%	1	1	1
Dry Cooling	1%	2.5-5	0	0
Hybrid Cooling	??[1]	2-4	0.2-0.7	0.25-0.5
Cooling Ponds	~14%[1]	Site Specific	~1[2]	~1[2]

1.2.2 SCO_2 as the Working Fluid in a Natural Circulation Decay Heat Removal System for Nuclear Power Plants

As the latest technology to be presented for nuclear power, proponents of SMRs often discuss their inherent safety features. One area of safety that is specific to nuclear power is that of decay heat removal. Unlike other power generation sources, when a nuclear power plant is shut down, it continues to generate heat. This heat is called decay heat and is chiefly generated from two sources: beta decay of fission fragments and gamma decay of fission fragments. The decay heat power level varies with the operational history of the reactor and decays approximately as:

$$P_{\tau}(T) \propto (\tau - T)^{-1.2}. \quad (1)$$

In proportionality (1), T is the time during which a group of fission events occurred and τ is the time at which one is observing the heat being produced. In order to find the total power level at a given time after shutdown, this relationship would need to be integrated over the entire power history of the reactor, and then evaluated at time τ. Letting T_0 be the time at shutdown and defining t as the time since shutdown, the decay power level at time t since shutdown can be calculated for a given reactor power history (2). Calculating the fission rate per MW of power and converting the decay energy produced for each fission event into the appropriate units, one arrives at the following expression for decay power after shutdown.

$$P(t) = P_0 \times 0.066 \times [t^{-0.2} - (t + T_0)^{-0.2}] \quad (2)$$

[1] Tsou, et al, list Cooling Ponds as 14% and do not list statistics for Hybrid Cooling at power generation plants.
[2] Cooling ponds store water for use in a Once-Through or Wet Cooling Tower System.

Equation (2) is valid from 10 seconds after shutdown to about 100 days after shutdown, with t measured in seconds. If one assesses the value of the power at one second after shutdown for a reactor with a constant power history of P0 for one year, the result is about 6.3% of P_0.

The total decay energy released grows as approximately t0.8 for the first months after shutdown. This energy is deposited in the fuel and surrounding structural materials of the reactor if there is no coolant to remove this heat. Over a period of time, this heat will cause drastic damage to the core, releasing large amounts of radiation to the environment and causing copious amounts of economic damage in the process. For this reason, nuclear power plants must have a means of removing this decay heat should an event occur that causes an unplanned shutdown of the reactor. The decay heat removal system serves this purpose in reactors.

An ideal nuclear decay heat removal system would have the following characteristics:

1. 100% reliable.
2. Capable of removing the decay heat at the maximum rate at which it is produced.
3. Capable of removing all the decay heat that is potentially available to be produced.
4. Requires no source of power other than the decay heat that is being removed from the reactor.
5. Requires no human interaction for initiation and/or operation.
6. Does not drain any power from the reactor when the decay heat system is not in use.
7. Impervious to malicious attacks.
8. 100% passively safe.

While it is not likely that any decay heat removal system will meet all of these characteristics, sCO_2 has characteristics that indicate it would be an improvement over other decay heat removal working fluids in some areas. This is particularly true for numbers four and five above. The reason for this is that sCO_2 has properties that make it easy to induce natural circulation in a loop that is designed correctly.

Natural circulation – in an engineered system – is a phenomenon in fluids whereby the fluid can be induced to flow without use of a pump or compressor to add energy to the fluid. In natural circulation, a fluid in an enclosed loop is heated at one point and cooled at another point in a configuration that creates a density difference; this density difference is then utilized to force circulation in the loop by utilizing the difference in the gravitational forces on the fluid. The driving force is then proportional to the difference in densities and also proportional to the height difference between the cold portion of the fluid and the hot portion of the fluid. This is illustrated in Figure 9 [14].

Different fluids have different propensities for initiation of natural circulation. The most important property for a natural circulation candidate fluid is a large change in density over the temperature range of interest. Ideally, this change in density will occur over a small temperature difference. The reason for this is that it is easier to engineer a system over a small temperature range than to engineer a system over a large temperature range, due to multiple factors, including materials issues and thermal stresses. One measure of a fluid's propensity for natural circulation is the Grashof number (Gr). The Grashof number is a dimensionless number that approximates the ratio of buoyancy to viscous forces in a fluid. For a pipe, the Grashof number is:

$$Gr = \frac{g\beta(T_w - T_B)D^3}{\upsilon^2} \tag{3}$$

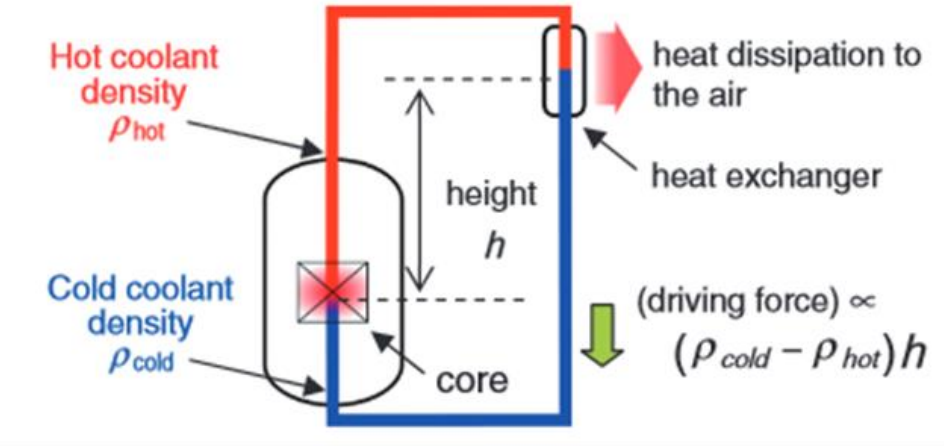

Figure 9 Illustration of natural circulation configuration [14].

For sCO_2, the value of Gr near the critical point indicated that it is more conducive to natural circulation than water. Table 1 compares the Grashof numbers of water and CO_2 divided by the cube of the characteristic length at a bulk temperature of 300 K, a wall temperature of 310 K and pressure of 7.69 MPa. This is very near the critical point of CO_2, which occurs at a temperature of 304.1 K and a pressure of 7.38 MPa [11]. Although the Grashof number is not the only factor to consider when evaluating a fluid for potential use in a naturally circulating decay heat removal system, the fact that this number is four orders of magnitude greater than that of water in this regime makes if worth investigating.

The combination of the natural circulation capability of sCO_2 and the ability to utilize dry heat rejection for the transfer of heat makes CO_2 an ideal candidate for further investigation of its potential for use in aSMRs.

Table 2 Comparison of Grashof numbers of water and CO_2 divided by characteristic length cubed, assuming ΔT of 10 K [11].

Parameter	Units	CO_2	Water
Bulk Temperature	K	300	300
Pressure	MPa	4.69	7.69
β	1/K	0.039	0.00037
ρ	kg/m^3	275.6	996.7
μ	Pa-s	2.21e-5	6.94e-4
Gr/Lc^3		5.9e14	7.5e10

1.3 Report Content

This report serves to document the reasons that Sandia National Laboratories funded this LDRD project and reviews the work completed. It also outlines the results and conclusions drawn from this work. The

report is divided into five sections. Section 1 is the introduction and background, which provides the motivation for this work and some background information to help the reader understand the work. Section 2 provides a description of the experimental apparatus, including the two different configurations and why they were used, as well as the major components required to build and operate the apparatus. Section 3 describes the experiments that were performed and presents the results as well as the analysis of these results. Section 4 describes the computational fluid dynamics (CFD) models that were developed for prediction of the results and for scaling of this type of experiment to larger sizes. Section 5 provides conclusions and further work that is needed.

2 DESCRIPTION OF EXPERIMENTAL APPARATUS

This section of the report describes the physical setup of the experimental sCO_2 natural circulation loop. There are two subsections in this section because the loop was operated in two different configurations.

In the first configuration, the CO_2 was heated via a water-to- CO_2 heat exchanger and cooled with an Xchanger CO_2-to-air heat exchanger.

In the second configuration, the CO_2 was heated via an induction heater and cooled via a single-pass tube and shell (or concentric tube) CO_2-to-water heat exchanger.

2.1 Water-Heated, Air-Cooled Natural Circulation sCO2 Loop

In the first operational configuration of the sCO_2 natural circulation loop, a Keltech Acutemp 50 kW heater was used to heat water. The water was then passed through the shell side of a Sentry spiral heat exchanger. The sCO_2 was then cooled via an Xchanger CO_2-to-air heat exchanger. Figure 10 is a picture of the water heater. Figure 11 is a picture of the spiral heat water-to-CO_2 exchanger. Figure 12 is a picture of the CO_2-to-air heat exchanger. The loop utilized 1” OD Swagelok tubing with a 0.095” wall thickness. After the CO_2 passed through either of the heat exchangers, it passed through a Micromotion F Series Coriolis Flow and Density meter. There were also thermocouples before and after each heat exchanger to measure temperature and pressure of the CO_2. A MarwinValve 3000 Series adjustable valve was installed on the cold leg that could be used to increase flow restriction. Figure 13 is a schematic of the loop in this configuration.

This configuration was used principally to demonstrate that sCO_2 could be operated in a controlled, dry-cooled natural circulation loop. Prior to this LDRD project, there were no documented cases of this occurring.

Figure 10 Keltech Acute mp heater used to heat the water, which was then used to heat the CO_2 in the sCO_2 natural circulation loop.

Figure 11 Sentry spiral heat exchanger used to transfer heat from the water to the CO_2.

Figure 12 Keltech Xchanger CO_2 -to-air heat exchanger used in sCO_2 loop.

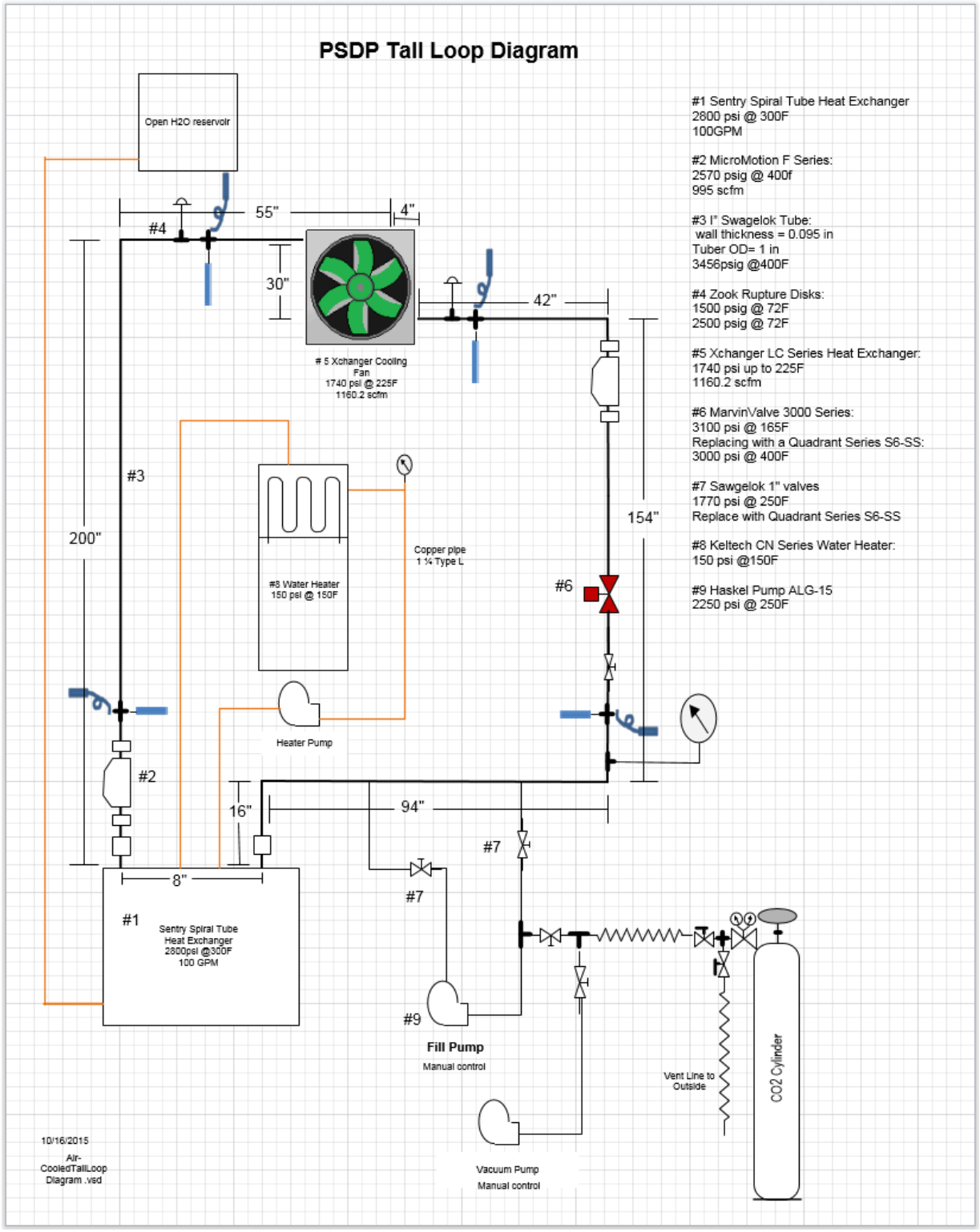

Figure 13 Diagram of the air-cooled, natural circulation sCO2 loop at Sandia National Laboratories.

2.2 Induction-Heated, Water-Cooled Natural Circulation sCO2 Loop

In the second operational configuration of Sandia's sCO_2 natural circulation loop, a Miller ProHeat 35 Liquid Cooled Induction Heating System was used to heat the CO_2. A concentric tube CO_2-to-water heat exchanger was designed and connected to in-house plumbing to cool the CO_2. Figure 14 is a schematic of the loop in this configuration. Table 3 documents the different components of the loop in this configuration.

This configuration was designed and implemented after demonstration of controlled, air-cooled, natural circulation of sCO_2 was established. The reason for this was to have the means of measuring wall temperatures of the tubes carrying the CO_2 so that engineering parameters such as Nusselt number, Grashof number, and Rayleigh number could be verified. However, some difficulties were encountered and the results that were obtained are preliminary at this point.

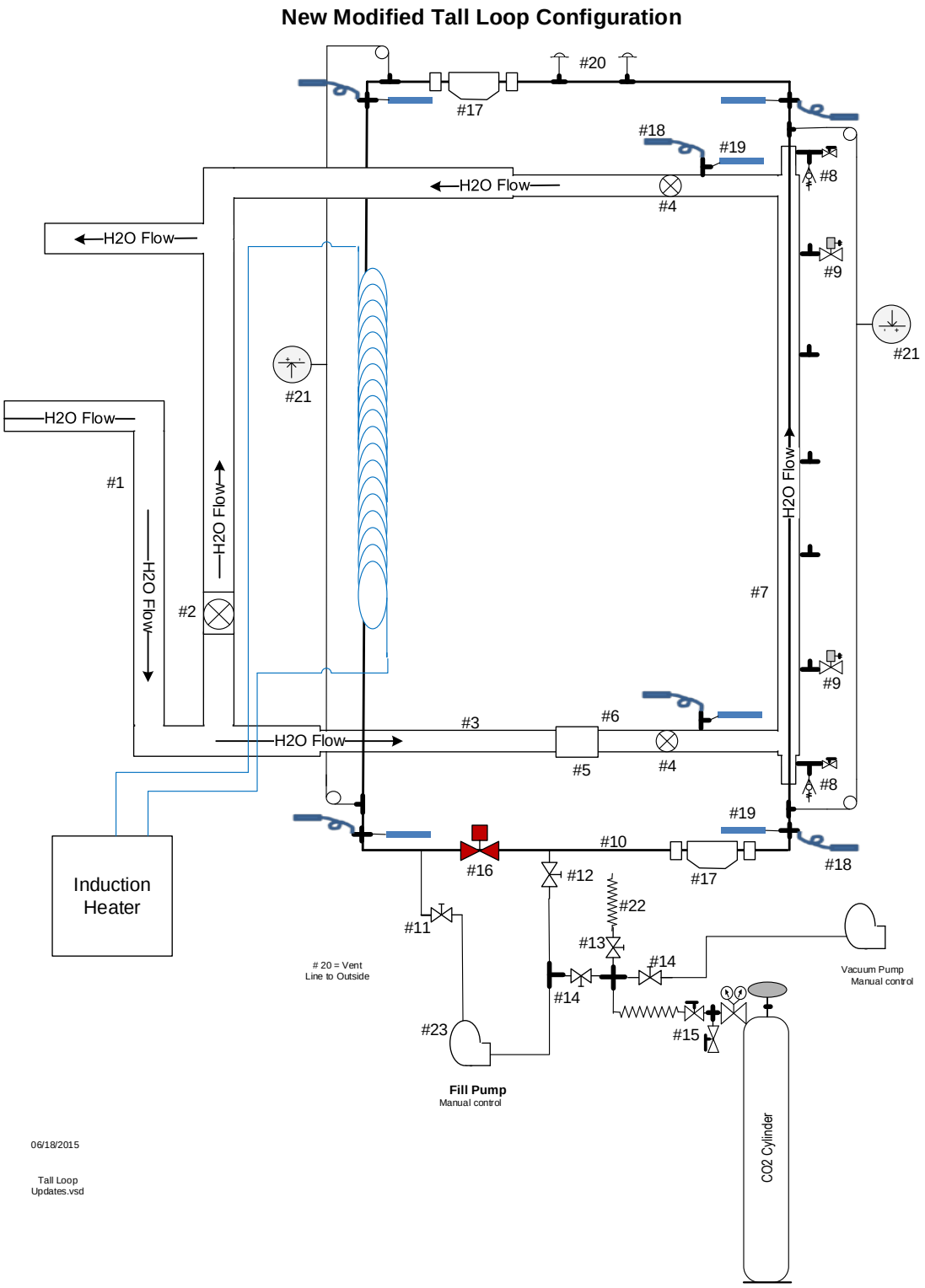

Figure 14 Diagram of the induction-heated, water-cooled, natural circulation sCO2 loop at Sandia National Laboratories.

Table 3 Parts list for induction-heated, water-cooled natural circulation loop at Sandia National Laboratories.

Water Cooling System = max flow rate of 150 gpm			
Part		**Pressure Rating**	**Temp Rating**
1.	3" Schedule 80 PVC	370 psi 148 psi	@ 73°F @ 160°F
2.	GF Type 317 Valve (bypass valve)	150 psi	@ 73°F
3.	2" Schedule 80 PVC	400 psi	@ 73°F
4.	GF Type 546 Ball Valve	150 psi	@73°F
5.	GPI Flow Meter w/remote mounted electronics	300 psi	@70°F
6.	2" Copper Type L Tube	315 psi	Up to 150°F
7.	2" Schedule 40 Stainless Steel Pipe	1902 psi 1474 psi 1355 psi	@ 100°F @ 300°F @ 400°F
8.	SS-RL4M8F8 Proportional Relief Valve (PRV)	Set @ 125 psi	Up to 300°F
9.	Solenoid Valve (1/2 inch)	250 psi	-40 to 220°F
CO_2 Loop			
Part		**Pressure Rating**	**Temp Rating**
10.	1" Swagelok SS Tube 0.095 wall thickness Swagelok Tube Fittings are rated to the working pressure of the tubing.	3600 psi 3600 psi 3456 psi 3060 psi	Up to 100°F @ 200°F @ 400°F @ 600°F
11.	SS-AFSS8 Swagelok valve (Loop Isolation)	6000 psi	@ 250°F
12.	SS-AFSS16 Swagelok valve (Loop Isolation)	4653 psi	@ 250°F
13.	SS-42GS4 Swagelok valve (vent to outside)	2500 psi	@ 300°F
14.	SS-43GS4 Swagelok valve	2500 psi	@ 300°F
15.	SS-43GM4-S4 Swagelok valve (At the regulator)	2500 psi	@ 300°F
16.	Quadrant Series S6-SS Valve	6000 psi 4500 psi 3000 psi	@ 100°F @ 250°F @ 400°F
17.	Micro Motion F-Series Coriolis Flow and Density Meters	3600 psi 3095 psi 2795 psi 2570 psi	@ 100°F @ 200°F @ 300°F @ 400°F
18.	Honeywell Pressure Transducers	3000 psi	185°F (on pigtail standoff)
19.	Conax RTD		Up to 1122°F
	Omega Type K Thermocouples (TCs)		2282°F

20.	Zook Rupture Disks	2500 psi	@ 73°F (on standoff)
21.	Kobold Differential Pressure Transmitters	4499 psi	-40 to 248°F -40 to 176°F (ambient)
22.	Swagelok tube for venting Swagelok flex hose (for filling and venting) Could be PFA tube vent line (-320 to 500°F, 4700 psi)	3700 psi 3100 psi 4700 psi	-20°F to 100°F -325°F to 850°F -320°F to 500°F
23.	Haskel Fill Pump (2250 psi up to 250°F)	2250 psi	@ 250°F
24.	Flexible Tear-Resistant Silicone Foam Pipe Insulation		-100°F to 500°F

3 Experiments performed

3.1 Air-cooled configuration

Multiple experiments were performed in the air-cooled configuration (see Section 2.1). This section reviews these experiments. Prior to October 16th, 2014, some short tests were performed. These original tests were conducted primarily as shakedown tests.

Leak-testing and control/data acquisition verification were performed over a period of months during the summer of 2014. Engineered safety concepts were implemented during construction and shakedown testing. After all control and safety concerns were addressed, testing began in October, 2014.

3.1.1 Boundary Tests Conducted on October 16th, 2014

On October 16th, 2014, the water-heated, air-cooled configuration was operated to determine the general values that could be expected during any given operation. The idea behind this test was to allow the operators to understand the general parameters that could be expected when operating the loop. The loop was operated for nearly five hours. During most of the test, the CO_2 was in the 2-phase regime.

Although for much of the test, the temperature difference between the hot leg and cold leg was approximately constant, the mass flow rate decreased during this time. No leaks were found in the system. It is believed that the measured mass flow decrease is due to the inability of the Micromotion flow meter to measure flow rate correctly in the 2-phase regime. This was not considered a major setback since the purpose of this particular project was to investigate CO_2 in the supercritical state. Further work will be completed in this regime.

3.1.2 Startup from 2-Phase Testing on November 4th, 2014

On November 4th, 2014, the loop was started with the CO_2 in the two-phase regime. While operating the loop, the measured flow rate was negative for part of the time and even when it was positive, the flow rate was very low. The temperature was also higher at the point where the CO_2 should have been leaving the cooler instead of where it should have been entering the cooler. The only reasonable explanation for these observations is that the CO_2 was circulating in the opposite direction from what was expected. This is conceivable because the water-to-CO_2 heat exchanger was positioned in such a way that the CO_2 could flow out of the heat exchanger in either direction. Figure 16 shows the CO_2 temperature entering the cooler and leaving the cooler, as well as the measured mass flow rate. Also included is a first-order approximation of the heat rate, assuming a constant specific heat capacity through the air cooler. Note that for much of the first portion of the experiment, the “Cooler Out” temperature is greater than the “Cooler In” temperature. Initially, it was thought that restricting flow to the cold leg before startup by partially closing the MarwinValve might cause flow to initiate in the preferred direction. However, this did not prove to be the case. Heat to the loop was suspended after about an hour and a half. The loop was monitored to ensure that no safety issues occurred.

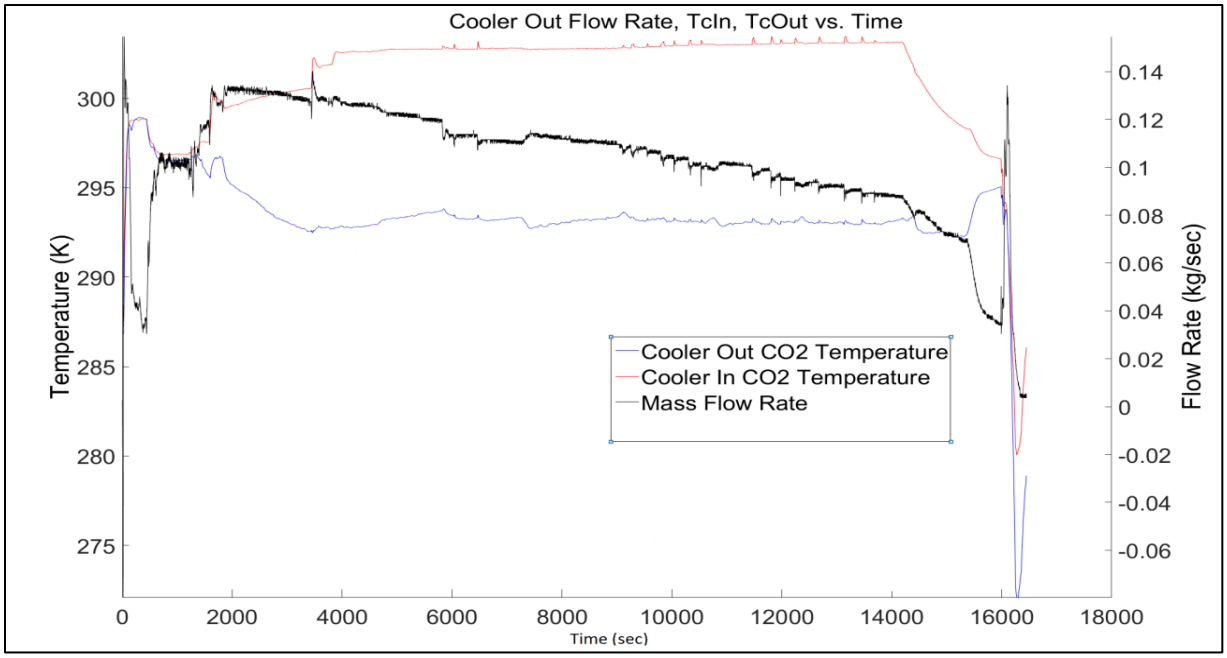

Figure 15 Mass flow rate and temperatures observed in first test after shakedown.

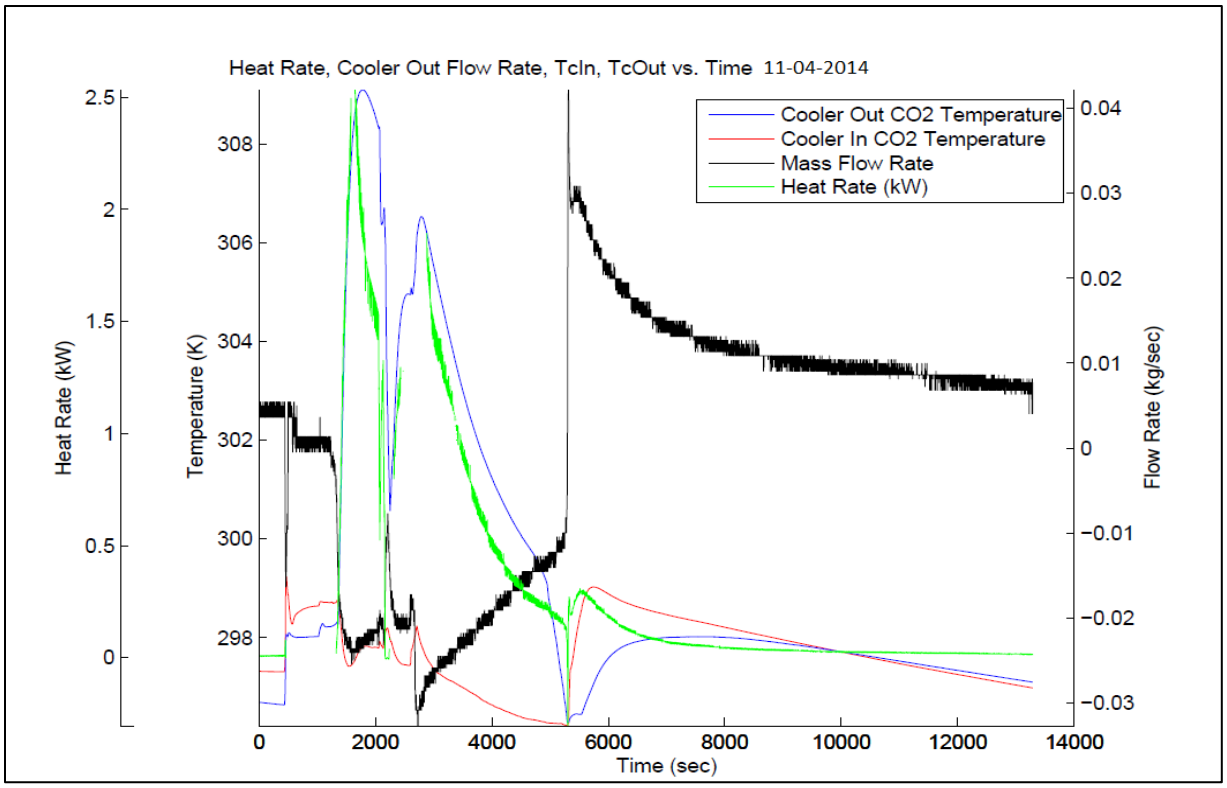

Figure 16 Results from starting up from 2-phase regime. The negative values of flow rate indicate reverse flow. The heat rate assumes constant C_p and is not reliable for this regime.

3.1.3 Startup from 2-Phase Testing on November 5th, 2014

On November 5th, 2014, the experimental team again started the loop while the CO_2 was in a two-phase state. This time, the fan on the cooler was turned on high before the loop was heated. The rationale behind this methodology was to create a cold slug of water at the top of the leg that is identified as the cold leg. This approach worked well and no evidence of reverse flow was identified.

After the initial startup phase, mass was added in step increases while maintaining a relatively constant hot leg temperature. This addition of mass was performed so that the response of the system could be monitored and also to gain information to validate the model that was used to estimate temperature and pressure for a given mass loading. As can be seen from Figure 17, the mass flow rate and the cold leg temperature increased with each mass increase (from about 3000 second to about 10000 seconds).

Just after 10000 seconds, the fan power was increased, thereby cooling the cold leg of the CO_2 and increasing the mass flow rate again (Figure 17, from ~10000 seconds to about 12000 seconds). Although the CO_2 was cooled, at no point during this transient did the temperature drop below the critical temperature (304.1 K). However, both the cold leg and the hot leg were very near the critical temperature, where the density of CO_2 varies drastically with only a small change in temperature. Thus, the mass flow rate increased in this region. Figure 20 is a plot of temperature versus density for CO_2. Isobars and pseudocritical points are shown to show how density can change very rapidly with a small change in temperature near the critical point, but may change very slowly with temperature as the CO_2 is heated to a state far from the critical point.

At about 18000 seconds, the CO_2 had cooled to the point that step increases in power could be performed while maintaining the cold leg temperature at a relatively constant value. As can be seen from Figure 17, this had little effect on the mass flow rate. The reason for this can be seen from Figure 17 and 20. Although the hot leg temperature was increased, the density change was minimal. Figure 19 plots the pressures for this experiment. The pressure change between about 18000 seconds and 26000 seconds is from about 7600 kPa to about 8800 kPa.

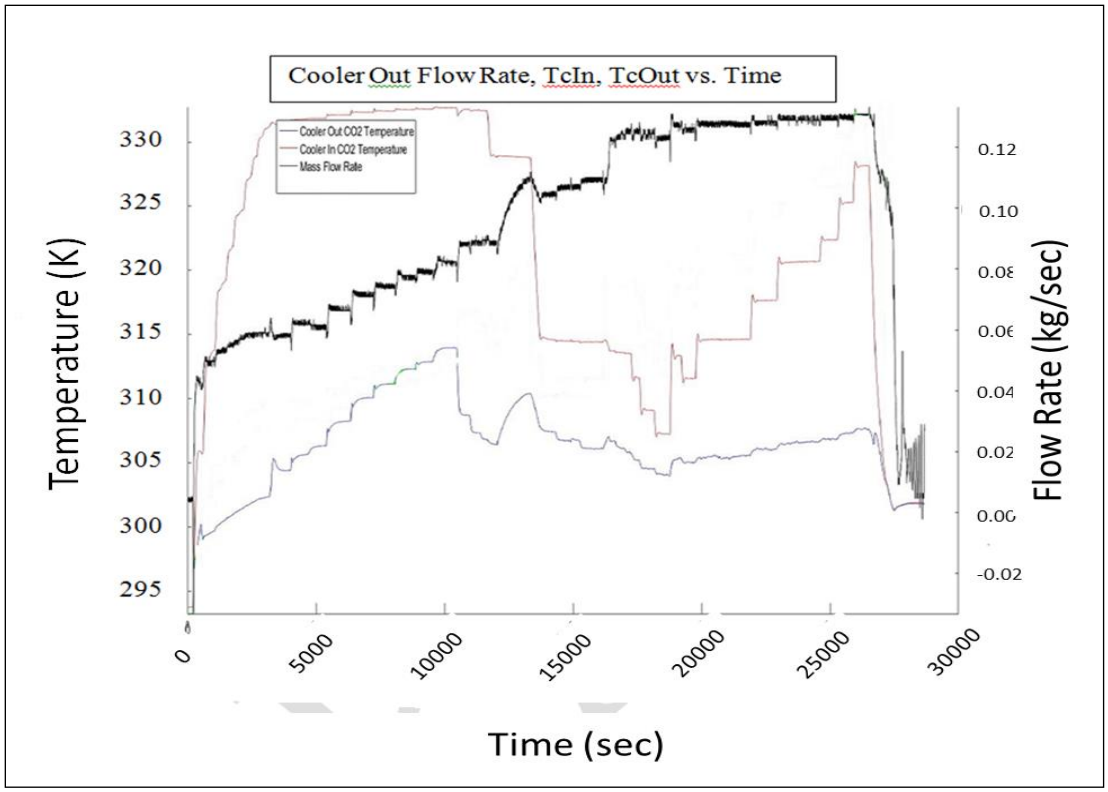

Figure 17 Plot of mass flow rate, hot let temperature, and cold leg temperature for experiment run on November 5th, 2014.

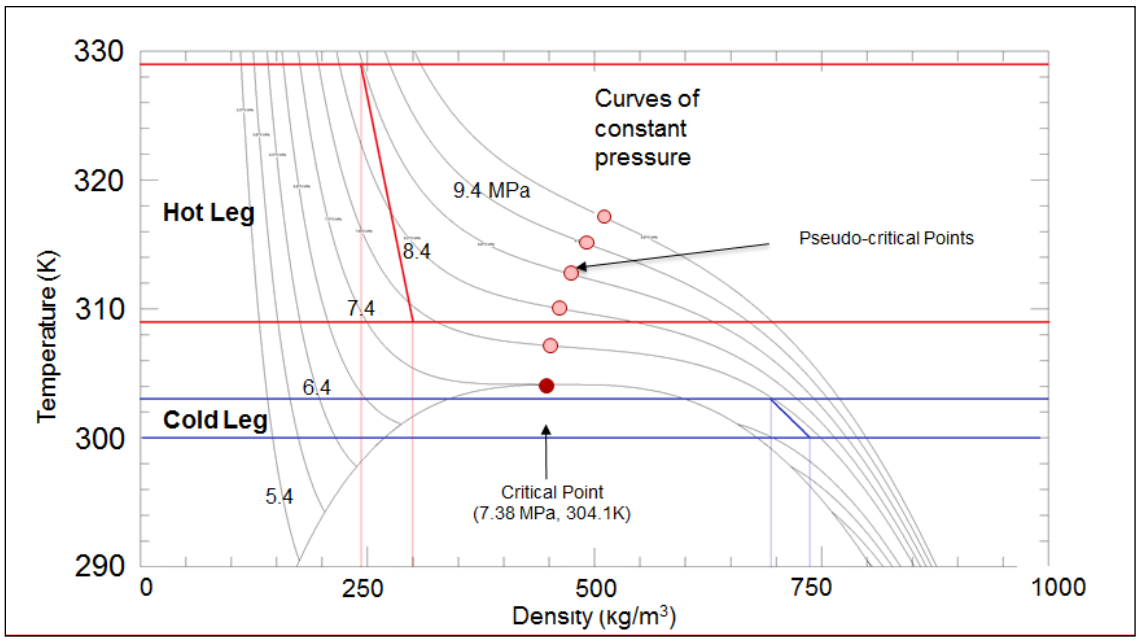

Figure 18 Temperature-density diagram for CO_2. The density changes rapidly with temperature near the critical point. However, further from the critical point, this is not the case. The red lines show a hypothetical change from 329 K to 309 K, with a corresponding.

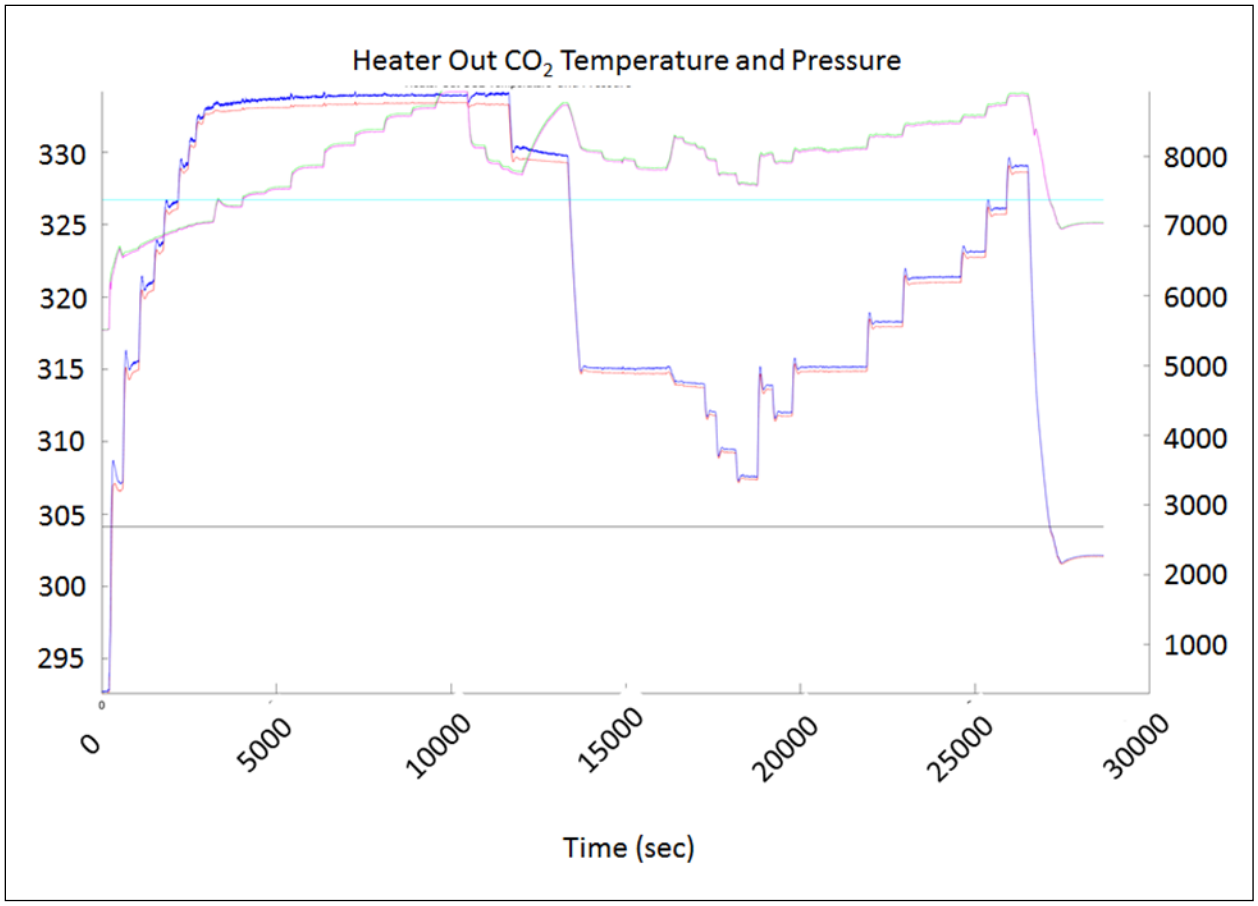

Figure 19 Temperature and pressure for the hot leg on November 5th, 2014.

3.1.4 Step Increases in Heating Power on January 16th, 2015

Due to the results from the November 5th experiment, another experiment was planned to verify that large increases in heat rate may not be accompanied by a correspondingly large increase in mass flow rate. On January 16th, 2015, this experiment was performed. The cold leg temperature was held relatively constant near the critical temperature by varying cooler fan speed. Hot leg temperature was increased in steps and allowed to reach steady state before being increased again. Hot leg temperature was varied in five steps from about 310 K to about 330 K. Figure 22 shows the results of the experiment.

Figure 21 marks the changes in temperature and pressure on a temperature-density diagram of CO_2. From about 6000 seconds to about 8500 seconds, the cold leg temperature dropped into the liquid state (below the critical temperature but above the critical pressure). This caused a large change in density for the cold leg, increasing the mass flow rate. However, from about 8500 second to about 13500 seconds, the cold leg was a liquid and ranged from about 300 K to about 303 K. The hot leg ranged in temperature from about 309 K to about 329 K, and in pressure from about 7800 kPa to about 8800 kPa. Thus, the hot leg density and cold leg density both change by about the same amount during this trial. As would be expected, the mass flow rate did not vary significantly.

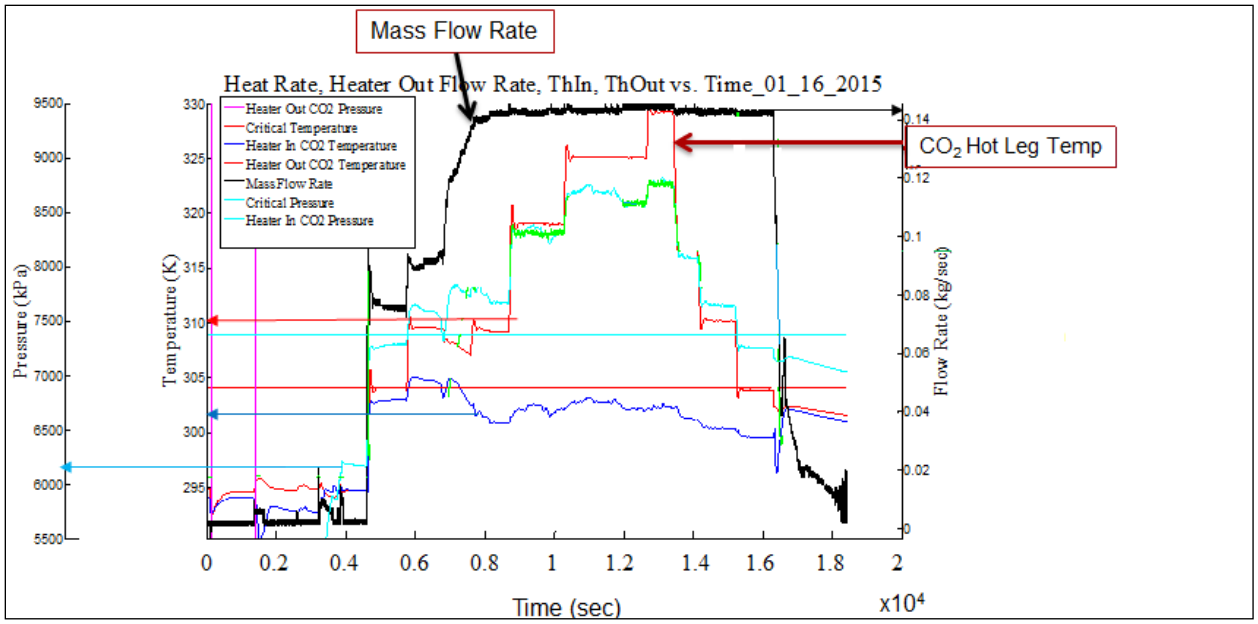

Figure 20 Results of January 16th, 2015 experiment to assess mass flow rate as a function of hot leg temperature change. Although the hot leg temperature changed by ~30 K, the mass flow rate changed very little due to the changes in hot leg and cold leg densities

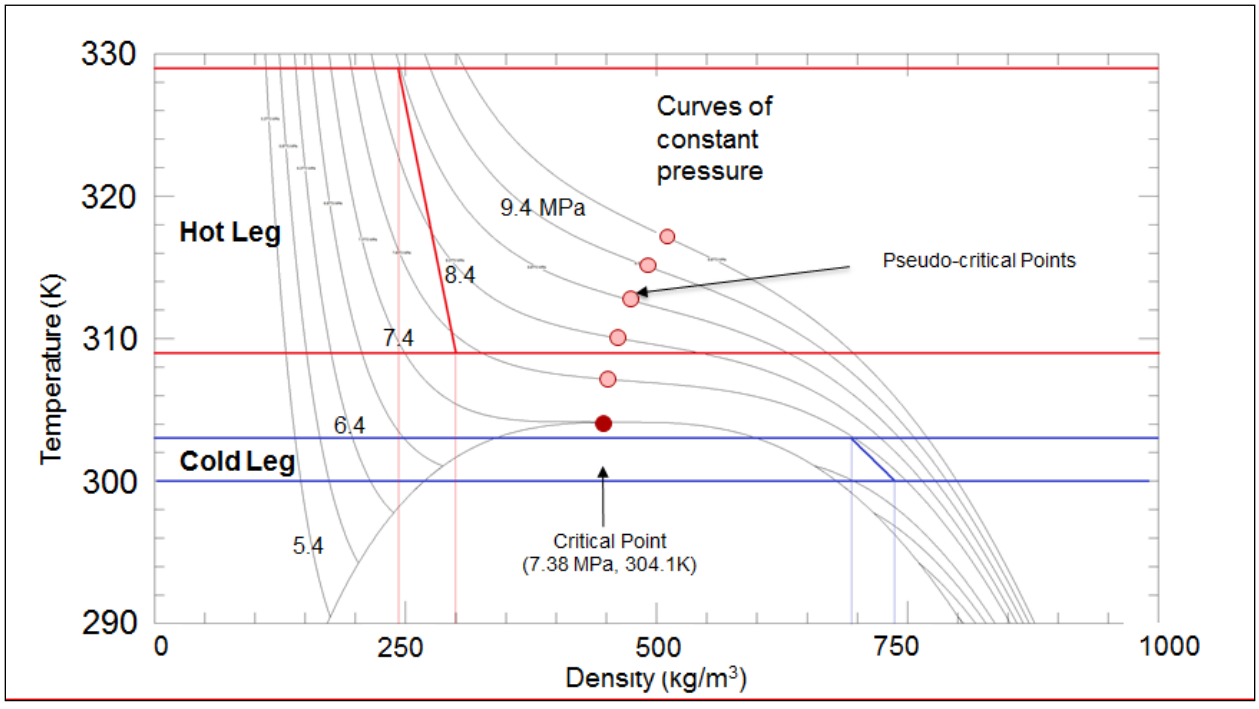

Figure 21 Temperature-density diagram for CO_2. The density changes rapidly with temperature near the critical point. However, further from the critical point, this is not the case. The red and blue lines show the regions within which the hot and cold legs of the natural circulation loop varied during step increases of power with on January 16th, 2015.

3.2 Induction-heated, water-cooled configuration

After the experiments in Section 3.1 were completed, focus shifted to gaining more basic scientific results as opposed to engineering and controls. The successful experiments in the water-heated, air-cooled configuration demonstrated that sCO_2 could be controlled and that the heat could be rejected by using air. The next step was to begin developing detailed information regarding heat transfer rates and flow characteristics. This information can then be combined with Computational Fluid Dynamics (CFD) codes and analysis of dimensionless numbers such as Nusselt number, Grashof number, Prandtl number, and Rayleigh number in order to make scaling calculations for real-world systems. In order to do this, a simpler design was needed.

Therefore, a Miller ProHeat 35 Liquid Cooled Induction Heating System was purchased. The maximum heating power of the Miller heating system is 50 kW. However, the actual heating power produced is dependent upon the strength of the magnetic field that can be induced in the metal. Finding a tubing that was the correct size and could safely operate in the sCO_2 environment while having a high enough magnetic inductance to ensure a large induced electric current is possible. However, this tubing is expensive and would require pressure testing beyond what was already performed for the loop that was in place. This would take more time than was available before funding ran out. Therefore, it was determined that utilizing the 1" OD Swagelok tubing that was already in place was the preferable option, even though it would limit the immediate tests to a maximum of 10-15kW. Two 20' sticks of 410 Stainless Steel pipe were ordered for future testing, but have not yet been installed.

Figure 22 is a conceptual design of the layout of the loop in this configuration. There are six thermocouples measuring wall temperature on the "hot leg" side of the loop. TC0 measures the wall temperature just before the CO_2 enters the region covered by the induction heater. TC1, TC2, TC3, and TC4 measure the wall temperature underneath the induction heater. TC5 measures the wall temperature just after the CO_2 leaves the heated region. On the "cold leg" side, the bulk water temperature in the heat exchanger is measured at five positions using resistance temperature detectors (RTDs). The CO_2 tube wall temperature is also measured at five positions using thermocouples.

Shakedown testing was performed on July 22nd, 2015. No problems were identified and experimentation began on July 23rd, 2015.

Figure 23 shows the water-cooled induction heating cable after it was installed on the hot leg of the loop. Figure 24 shows the CO_2-to-water heat exchanger before it was installed and Figure 25 shows the CO_2-to-water heat exchanger after it was hung but before it was connected to the rest of the plumbing.

One other improvement that was delayed due to expediency was the use of RTDs to measure outside wall temperature in the cooling region. Due to flow-induced vibrations, the uncertainty in these measurements was expected to be high. An alternative method of measuring this temperature is to use fiber optic sensors. This equipment was purchased but was delivered at too late a date to be installed and utilized in this project. It is expected that the equipment will be installed in the next year and more accurate measurements will be taken.

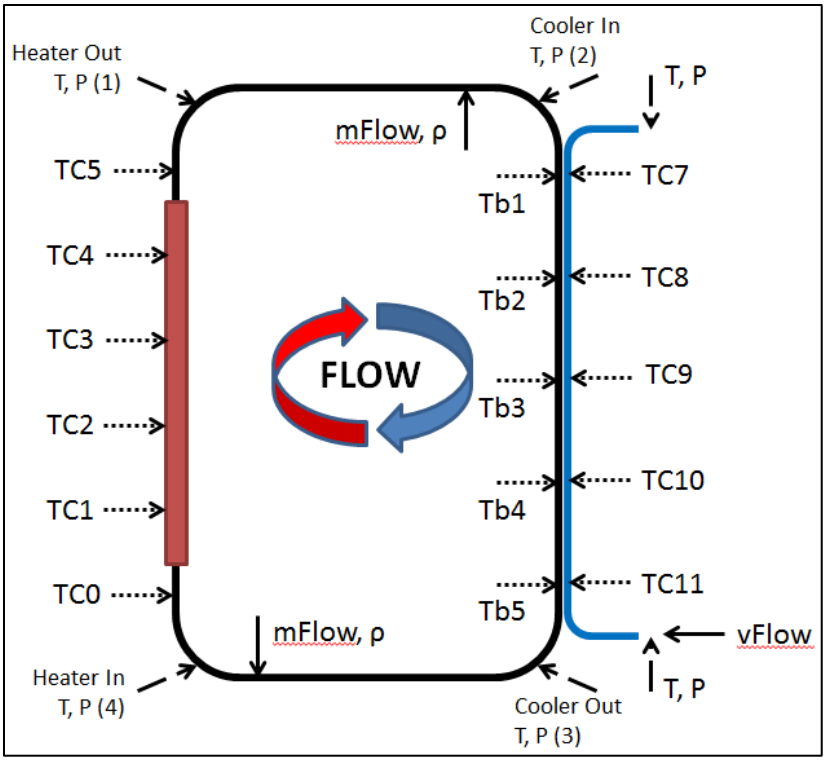

Figure 22 Diagram of loop in the induction-heated, water-cooled configuration.

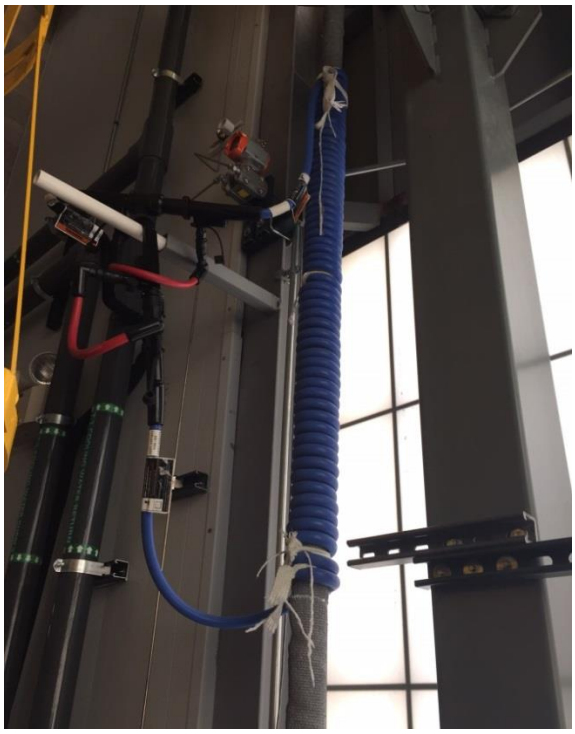

Figure 23 Water-cooled cable of the induction heater installed on hot leg of sCO_2 natural circulation loop.

Figure 24 CO_2 -to-water heat exchanger. The CO_2 passes straight through the center tube. The cooling water enters one flange and leaves the other.

Figure 25 CO_2-to-water heat exchanger.

3.2.1 Step Increases in Induction Heating Power on July 24th, 2015

This experiment focused on incrementally increasing the commanded power from the Miller ProHeat and comparing this with the actual power observed. It also focuses on observing the transient and steady-state behavior in mass flow rate due to these power increases. It was necessary to compare the commanded power with the observed power due to the use of austenitic stainless steel tubing which has a very low relative magnetic permeability, leading to a very low induced electrical current in the tubing. By measuring the temperatures and pressures into and out of the heater and the cooler, the state of the CO_2 could be determined. Using this and the measured mass flow rates, an energy balance could be used to determine the actual heat that was transferred into or out of the CO_2. Equation 4 was utilized for these calculations.

$$\dot{Q} = \dot{m} c_p (T_{exit} - T_{inlet}) \quad (4)$$

$\dot{Q}$ is the net heat into the fluid (may be either positive or negative).

$\dot{m}$ is the mass flow rate of the fluid.

c_p is the constant pressure specific heat capacity.

T_{exit} is the temperature of the fluid exiting the control volume.

T_{inlet} is the temperature of the fluid entering the control volume.

Figure 26 shows the Power levels observed for the experiment.

The mass loading, cooling water flow of 40 gpm, and cooling water temperature were kept constant through the run, with heating beginning around 640 seconds into the test. A commanded heat input of 2.6 kW to the Miller induction heater was supplied to initiate a flow of approximately 0.04 kg/s, as well as to increase the system pressure to just below the critical pressure of 1074 psi. The following three steps in power, to 4, 6.5, and 7.3 kW, show very similar trends in mass flow rate, pressure, and temperature. There is very little delay in transients between the hot- and cold-side of the loop due to its small size and thermal mass; however the steadying time for the cold-side of the loop is delayed by approximately 60 seconds from the hot-side due to the thermal mass of the water cooler.

Temperatures, pressures, mass flow, and heat transfer rates were very steady for each power level, with most showing an expected, almost logarithmic increase. However the mass flow rate displayed an interesting overshoot peak with each increase in power. This flow is driven under natural circulation by the difference in densities between the hot- and cold-sides of the loop; however, the overshoot is not reflected in the bulk temperature measurements. The overshoot then is likely caused by the transiently-increased hot-side wall temperature due to the fast response of the induction heater. This is understandable since the heating in the tube is not necessarily from outside in, due to the induction process.

Figure 27 shows the various temperatures pressures and heating rates observed in this experiment.

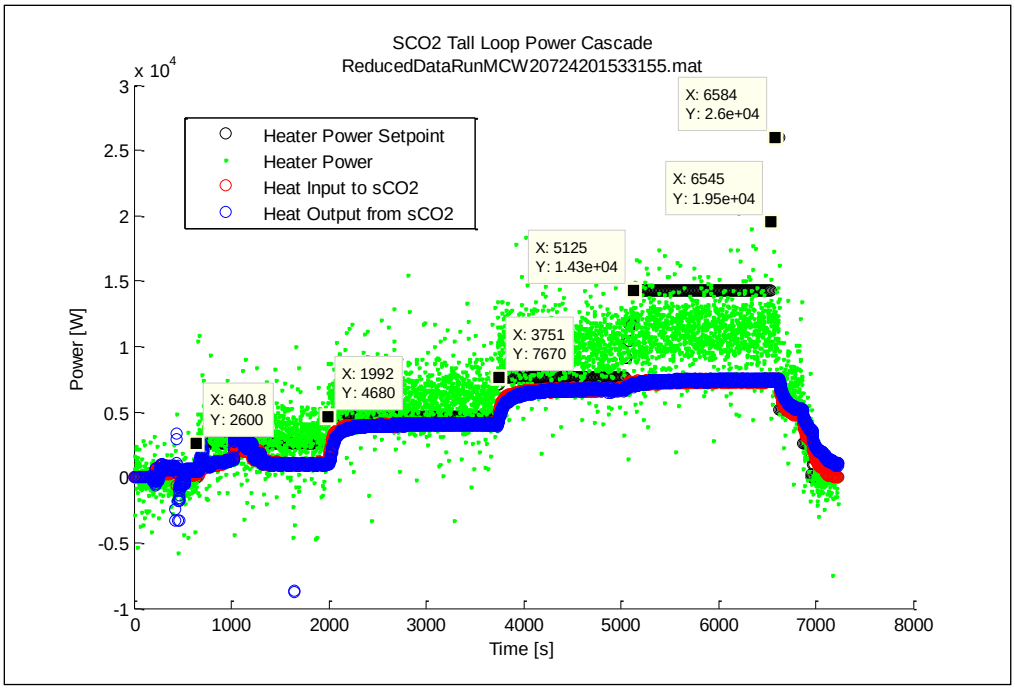

Figure 26 Power cascade for trial run on July 24th, 2015. The power levels observed in the heated section (red circles) and the cooled section (blue circles) were consistently less than the power commanded from the induction heater (black squares). This was expected because the tubing being heated was austenitic stainless steel, which has a very low magnetic permeability, resulting in very low induced electrical current. The green dots represent the instantaneous power reported by the induction heater.

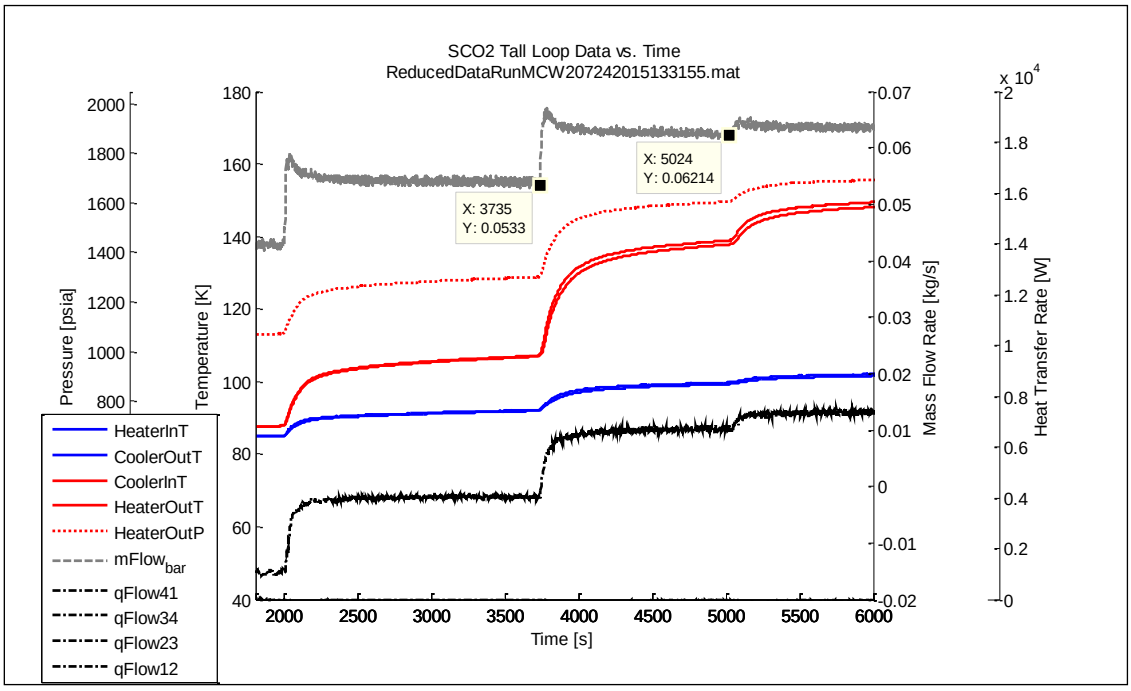

Figure 27 Temperatures, pressures, heating rates, and mass flow rate observed during step increases in induction power on July 24th, 2015. The overshoot in mass flow rate is thought to be caused by the transiently-increased hot-side wall temperature.

Figure 28 shows the measured wall temperatures at locations TC1-TC4 (Figure 22) as well as the CALCULATED bulk temperatures at those locations. Neither the wall temperatures nor the bulk temperatures show the overshoot that was observed in the mass flow rate (Figure 27). The calculated bulk temperatures show about an 80 K drop from the measured wall temperatures.

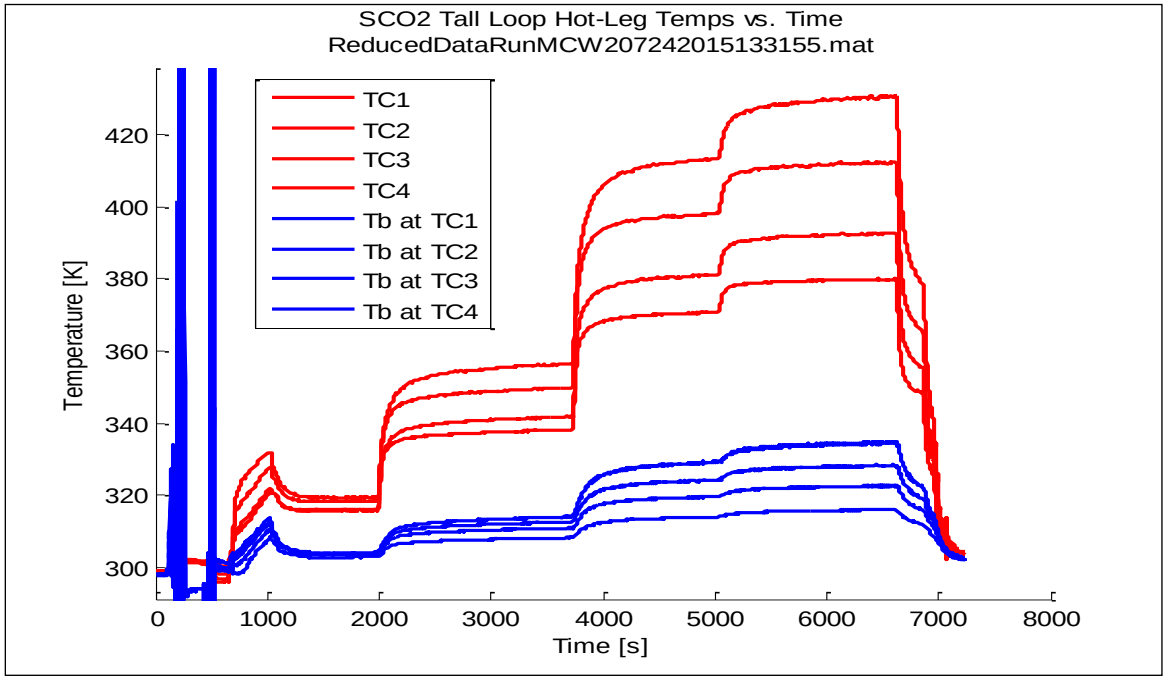

Figure 28 Measured wall temperatures (red) and calculated bulk temperatures (blue) in the heated region of the loop during step increases in induction heater commanded power on July 24th, 2015.

The trends in cold-side calculated bulk temperature show a nearly identical trend to the hot-side calculated and measured temperatures. The measured water temperatures and CO_2 tube outer wall surface temperatures are nearly identical, and trend upward over the course of the test a few degrees with ambient daily temperature changes. The close match between the measured wall and water bulk temperatures was expected due to the uncertain contact between wall temperature RTDs and the tube surface, as well as the stem effect on the RTDs passing through the cooling water stream extracting heat from the measuring tip. Future modifications to the loop should include insulation of these RTDs or alternative methods of sCO_2 bulk temperature measurements. Figure 29 shows the cold-side calculated bulk CO_2 temperatures, measured bulk water temperatures, and measured wall temperatures.

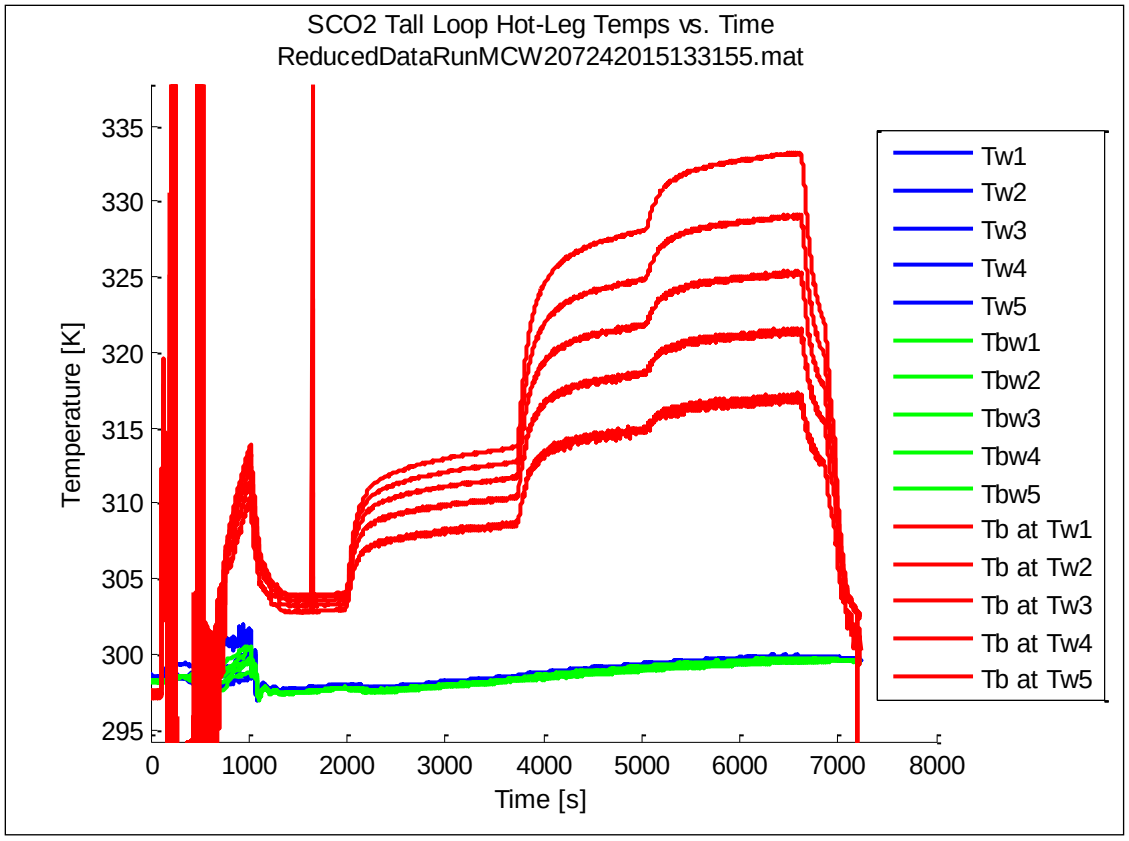

Figure 29 Cold-side measured wall temperatures (Tw1-Tw5), measured bulk water temperature (Tbw1-Tbw5), and calculated bulk CO_2 temperature (Tb at Tw1-Tb at Tw5).

More experiments and analysis are needed to fully understand the scaling factors that are needed for this type of loop.

4 Computational fluid dynamics (CFD) models

Both RELAP5 [15] and Fuego [16] were used to model the water-heated, air-cooled sCO_2 natural circulation loop because each provided a unique niche in terms of their computational ability, and tended to fill each other's gaps. In particular, the following are noted,

- RELAP5 advantages:
  - 2-phase flow
  - Strong validation and verification history
  - Built-in CO_2 properties
  - Fast
- RELAP5 disadvantages:
  - 1D momentum, mass, and energy transfer
  - Intended for large systems, therefore limited output
  - No explicit turbulence models
- Fuego advantages:
  - 3D momentum, mass, and energy transfer
  - Excellent turbulence and buoyancy models
  - Intended primarily for subsystems, therefore detailed output
  - Natural circulation has significant validation and verification (V&V), though not as much as RELAP5
- Fuego disadvantages:
  - 1-phase flow, which can be extended to "1.5"-phase flow
  - No physical properties; can use tables to overcome this, or can use Cantera
  - Slow, but can use massively parallel systems (1,000s to millions of processors)

4.1 Relap5 Model of the sCO_2 Natural Circulation Loop

The RELAP5 model considered 1D momentum, mass, and energy transfer. On the other hand, it computed two-phase flow in the form of liquid and gas, as well as the interfacial drag between the two. The code included CO_2 at the liquid, gas, and supercritical regimes. It was confirmed that the RELAP5 properties agreed with the fluid properties from NIST. Input line "1" (development model control) was used with flag 11, to enable the linear, rather than cubic, interpolation for the calculation of CO_2 properties near the supercritical point [15]; this flag is intended to make the code more robust.

The modeled system was under natural circulation as the heater lowered the fluid density, while the cooler increased the density, resulting in net flow of CO_2. The input model consisted of four pipes that

were connected by four single junction (singljun) connectors; see Figure 30. The singljun connectors included bend losses (K-factors) of 0.2, which were based on standard loses found in a standard fluid-loss handbook [17]. No additional losses were required to compare favorably with the experimental data as will be shown later.

The input model included two stainless-steel heat structures (HS) that were connected hydraulically on one side to the piping, and to the heat exchanger/cooler on the other side. In particular, the top HS modeled the cooler, and included a temperature vs. time table for the heater response. In the same fashion, the bottom HS modeled the heater, with another temperature vs. time table. Both tables were obtained from the experimental data, and set in a format that was readable by RELAP5. The experimental temperature history is shown in Figure 31. Note that from 0 to 4800 seconds, the cooler temperature was slightly hotter than the heater temperature. This was due to a calibration issue, but did not have an impact on the mass flow rate experimental data because the fluid velocity was nearly zero. However, near the supercritical point, small changes in pressure (and temperature) will have significant changes in density. Therefore, the first 4800 seconds for the experimental density are not considered reliable. The experimental data also indicates that from 13500 to 16400 seconds, the fluid adjacent to the heater started dropping, while the cooler temperature remained rather flat. This indicates that the mass flow rate should start decaying in response to the ever-smaller driver temperature difference, though the experimental data showed a rather flat mass flow rate up until about 16400 seconds. By that time, the cooler and heater had nearly identical temperature, so the mass flow rate should decay very rapidly beyond that point, as shown in the experimental data.

In order to calculate the correct heat transfer across the HS, effective heater dimensions (thickness, length, nodes, etc.) were chosen based on the estimation of heat transfer across the pipe-HS interface. This was based on the net heat flux across the lumped heater that was imposed (driven) by the temperature table. This established a uniquely-specified resistance across the HS, and once the heater dimensions were selected for the model, the code used the same values throughout the 18417 seconds of transient data. The HS had 20 nodes, with an effective thickness of 0.025 m.

The top and bottom pipes consisted of 10 volumes each with a segmental length of 0.259 m, while the two vertical pipes each had 20 volumes, each with a segmental length of 0.254 m. All pipes had a roughness of 1.5×10^{-5} m, which was relatively smooth. All segments had a hydraulic diameter of 0.0206 m.

All fluid velocities were initially set to zero, and the code was allowed to calculate the fluid velocity, density, and other primitive variables based on the temperature-vs-time forcing function from the experimental temperature data. The calculations were found to be temporally converged with a minimum and maximum time steps of 1×10^{-8} and 1×10^{-3} seconds, respectively. However, reasonably-converged faster results can be obtained with minimum and maximum time steps of 1×10^{-6} and 1×10^{-2} seconds. The implicit flag of 3 and 11 were found adequate for the calculations. Selection of minor edit variables was found ideal for comparison with the experimental data formatted into Matlab.

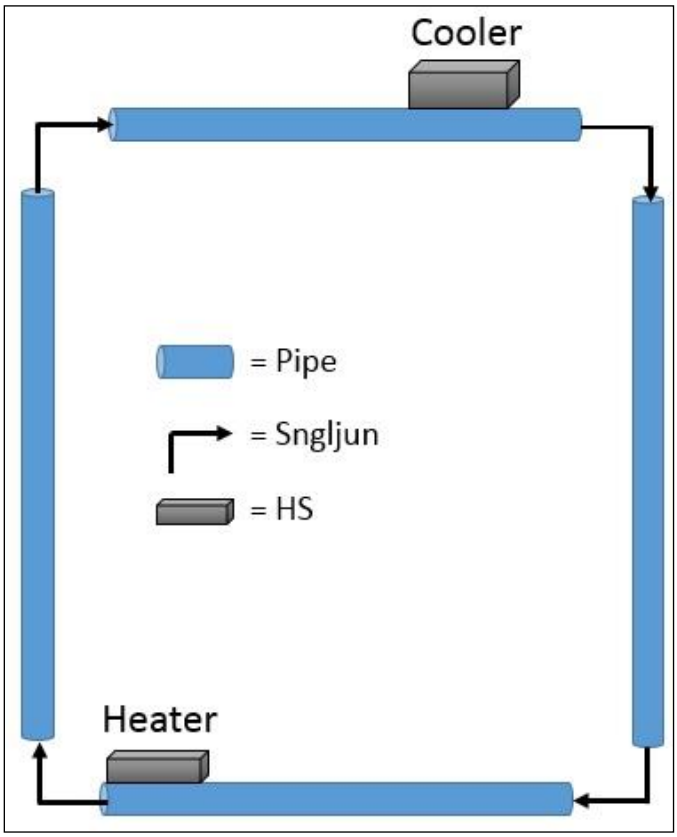

Figure 30 Schematic of RELAP5 SCO_2 Tall Loop Model.

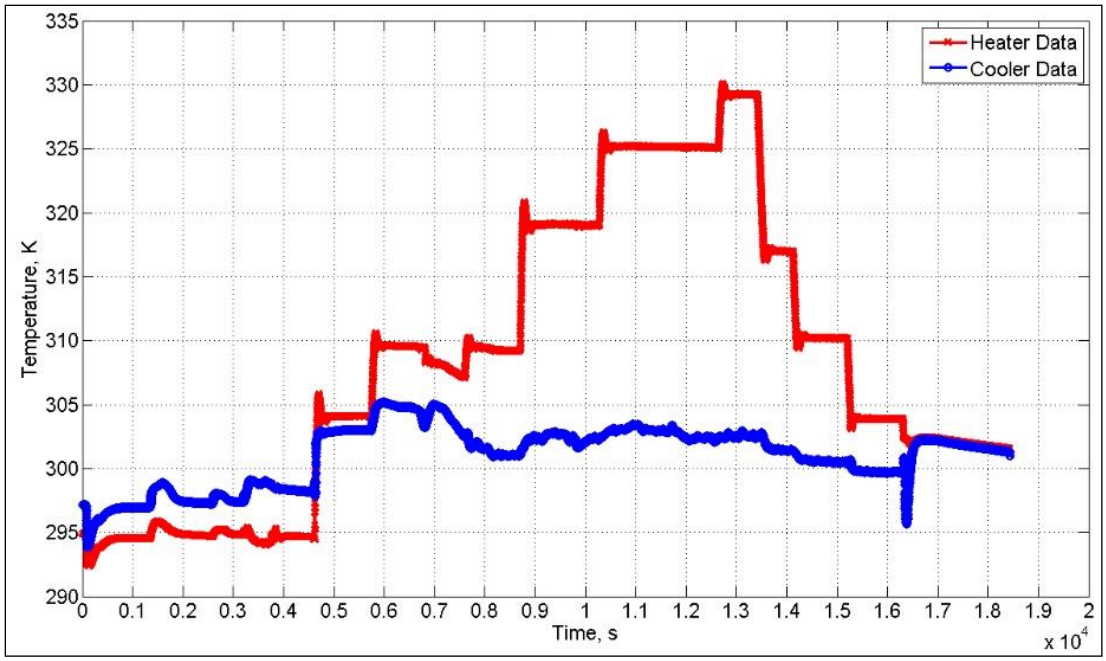

Figure 31 Experimental Temperature Data.

Figure 32 shows a comparison between the experimental mass flow rate experimental data and the RELAP5 output. It is noted here that from 0 to 15,000 seconds, most of the RELAP5 output was in excellent comparison with the experimental data, typically within 10% or less. For times greater than 15,000 seconds, the RELAP5 output decayed significantly faster than the measured values, primarily caused by instability in its density calculations; the RELAP5 output showed a steep rise in density (see Figure 35), which was likely precipitated by the steep heater temperature drop that occurred at about the same time in the experiment. This can probably be alleviated by decreasing the computational time step by a factor of 10 to 100, but was not done due to time constraints and because the transient was almost completed by that time. RELAP5 predicted the flow regime was two-phase, primarily in the bubbly (BBY) regime from 0 to 5,300 seconds, and thereafter was in the mist pre-CHF (critical heat flux) (MPR) regime for the duration of the simulation.

The RELAP5 density typically compared within 5% of the experimental data. The biggest discrepancy occurred at about 6,000 seconds, with about 12% error. That time period was also characterized by a sharp increase in heater temperature, followed by a fast overshoot in temperature. Again, this comparison could likely be improved by decreasing the time step, as discussed previously. It is very interesting that the sharp density magnitude oscillation experienced by RELAP5 was also shown in the experimental data, though within a much faster time period.

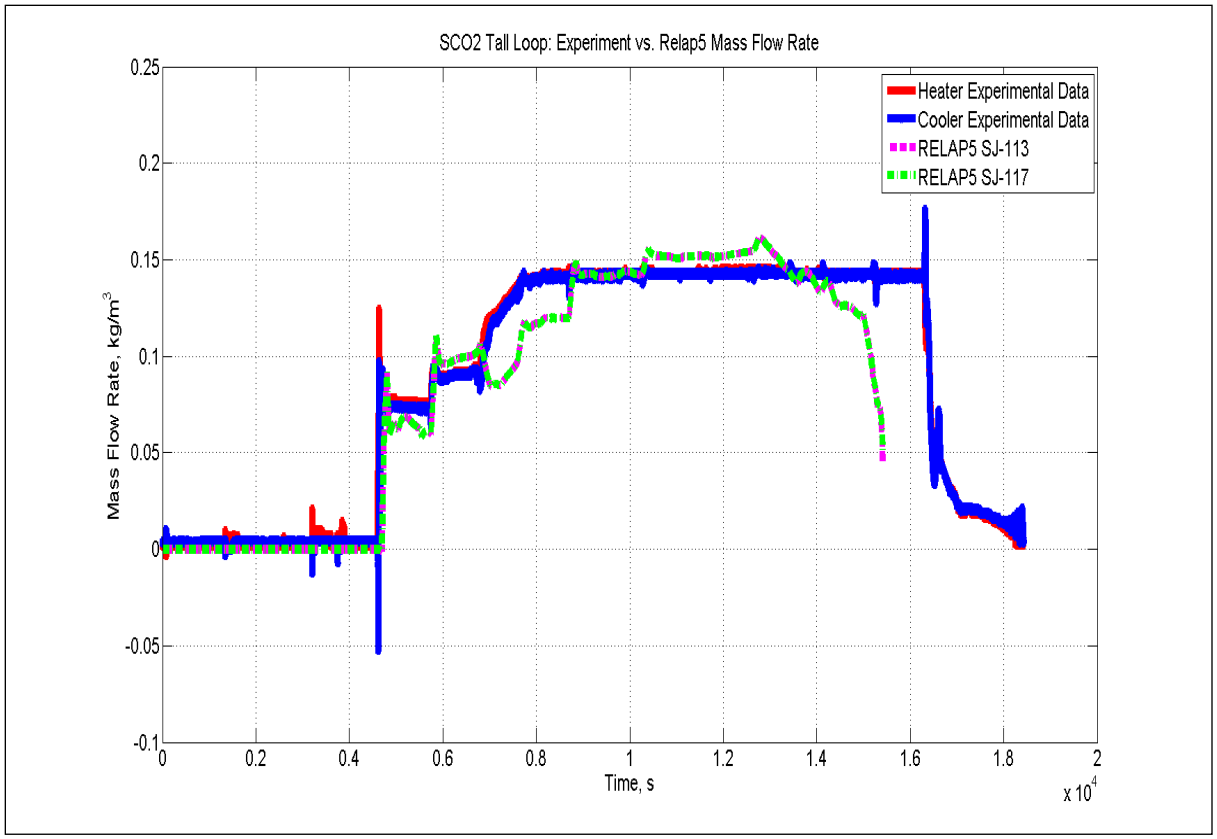

Figure 32 Experimental Data vs. RELAP5 output: Mass Flow Rate.

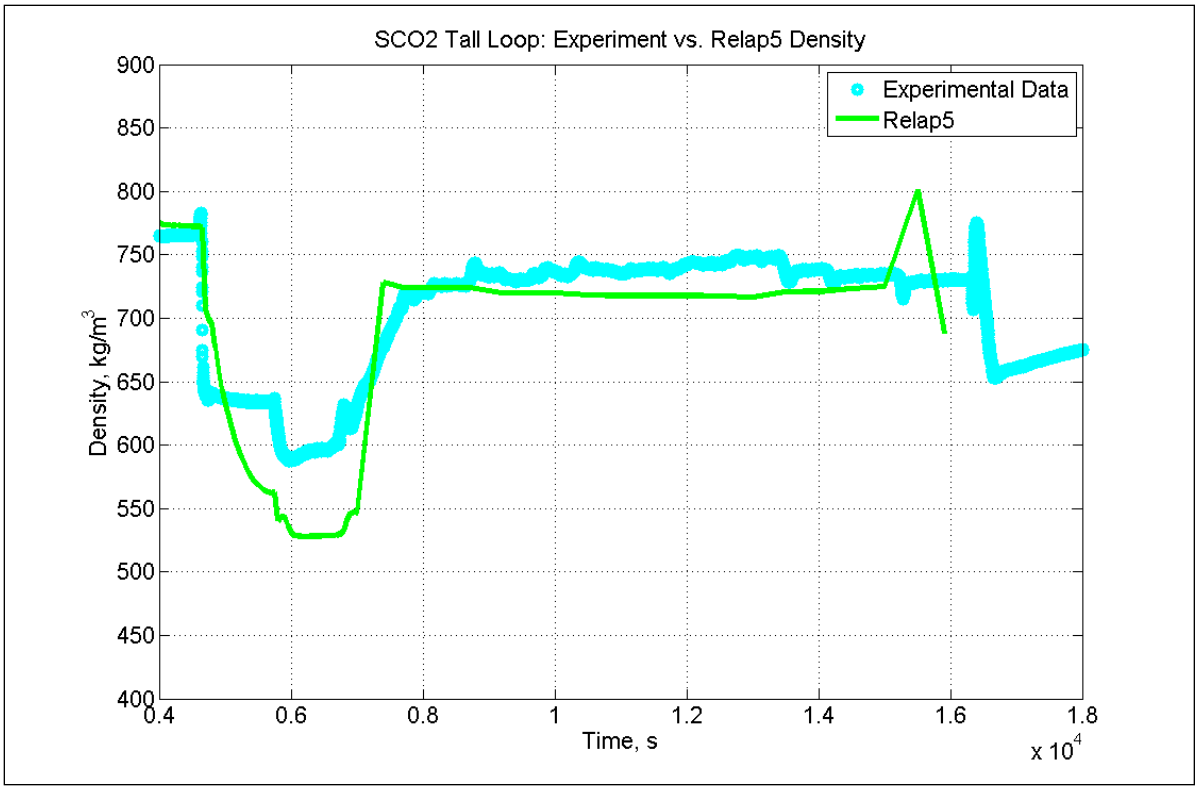

Figure 33 Experimental Data vs. RELAP5 output: Density.

4.2 FUEGO Model of the sCO_2 Natural Circulation Loop

The Fuego model considered 3D momentum, mass, and energy transfer. On the other hand, its material properties assumed the fluid was always at or above the supercritical point. However, Fuego can be "tricked" into modeling a two-phase fluid by inputting phase-averaged properties. The fluid properties were based on SCO_2 data from NIST. Fuego used the Boussinesq buoyancy model, and the large eddy simulation (LES) turbulence model. The entire piping geometry was modeled as shown in Figure 34, as well as a fast-running model that only included ¼ of the geometry. The heat exchangers were modeled with cooler/heater surface boundary conditions (BCs), with the top and bottom surfaces acting as BCs. Various meshes were constructed with 1.56, 3.11, and 6.27 million hex elements, thereby providing sufficient spatial convergence and good mesh metrics. A mesh segment is shown in Figure 35.

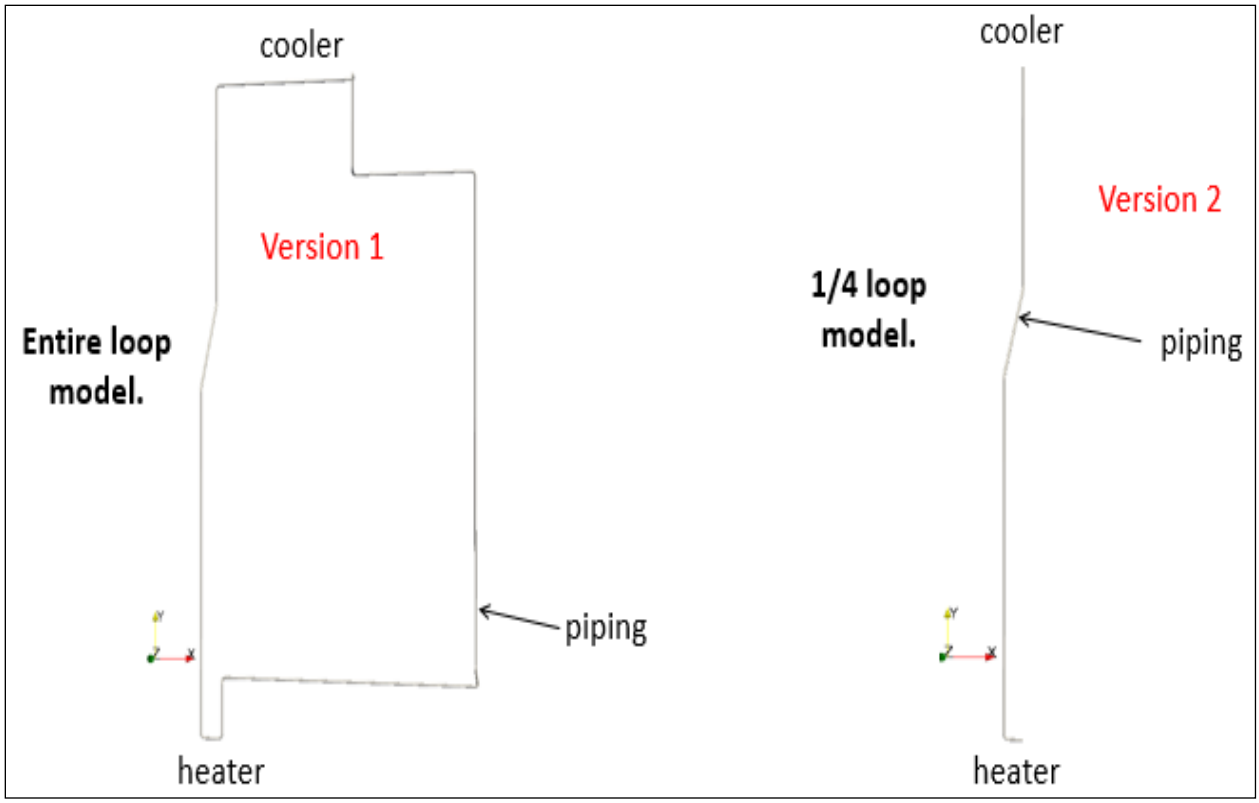

Figure 34 Schematic of Fuego SCO_2 Tall Loop Models.

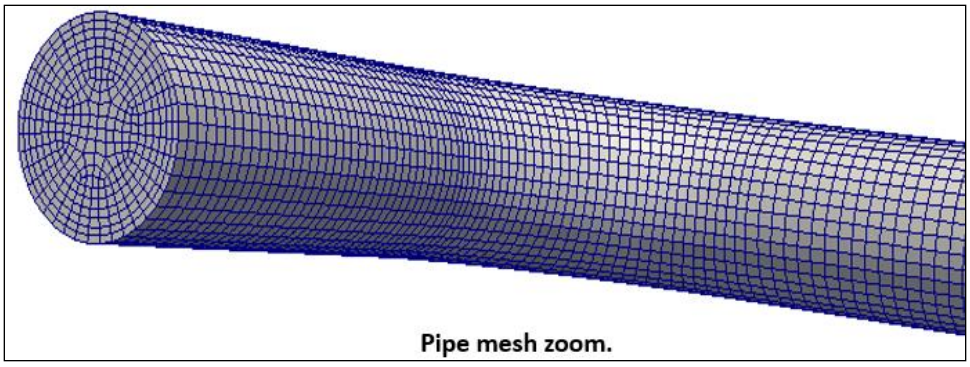

Figure 35 Mesh Segment for Fuego Pipe.

Figure 36 shows the temperature distribution in a pipe bend while the fluid is approaching its steady-state behavior, 10.7 seconds into the transient. The turbulent nature of the fluid can be observed in the vertical coherent structures captured by the LES turbulence model. The calculation revealed that the fluid traveled in clusters of fairly uniform temperature, but had wide temperature variations. This shows the importance of turbulence in the fluid; a high degree of turbulence will allow it to have more uniform temperature distribution, with improved heat transfer. The same issue is reflected in Figure 37, which shows the fluid distribution along a bend that has fully-developed flow. Of course, because the fluid is turbulent, it can never reach steady-state in the full sense of "no change with respect to time". That is, so long as the fluid is turbulent, there will be velocity fluctuations throughout the piping as a function of time. Steady-state

values can be obtained by performing time-averaging, if so desired. Figure 37 also shows large radial velocity gradients within the SCO_2.

It is noteworthy that having detailed, 2-phase/3D CFD output allows for a better-understanding of the SCO_2 behavior, how to efficiently scale SCO_2 systems, and provides an increased ability to transfer heat and momentum more efficiently, as will be shown in the next section.

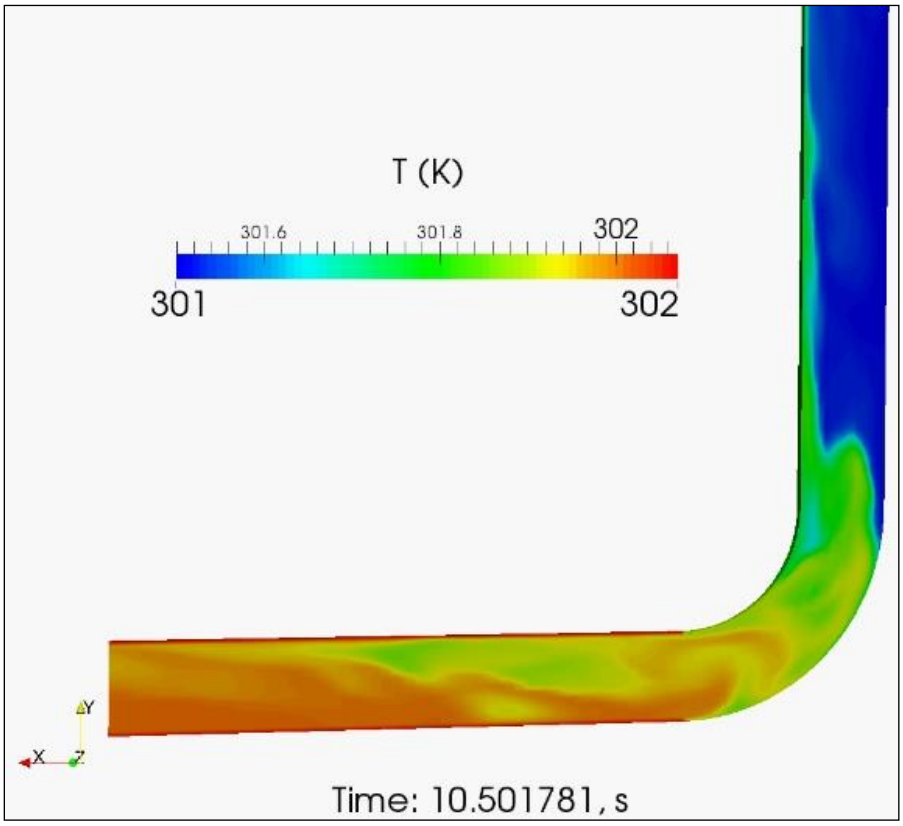

Figure 36 Temperature Distribution in a Pipe Bend as the Fluid Approaches Steady-State.

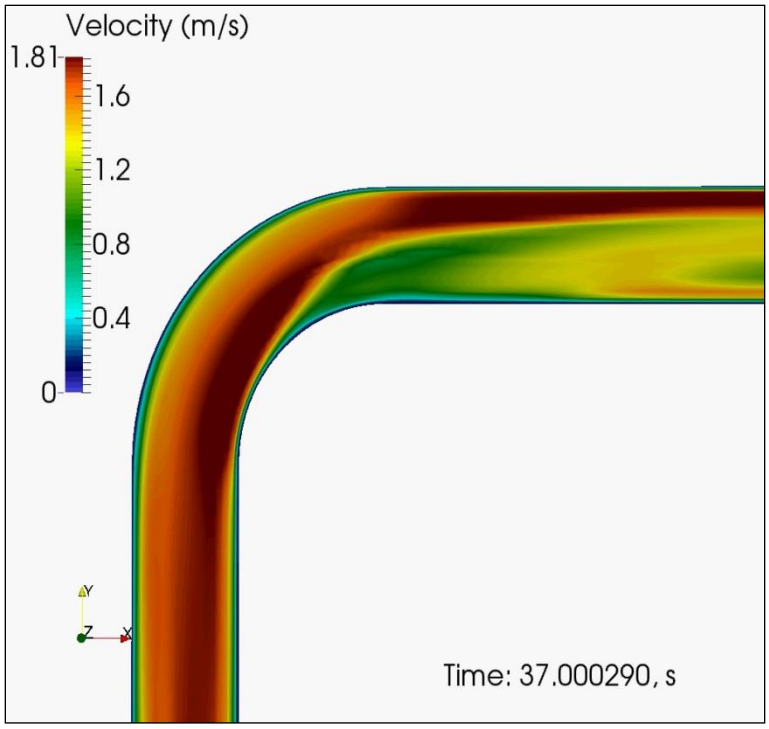

Figure 37 Velocity Distribution in a Pipe Bend.

Scaling, Increased System Efficiency, and Dimensionless Parameters

By considering key dimensionless parameters involved in natural circulation, important fluid dynamics and heat transfer characteristics can be gleaned, which provide enormous guidance for scaling the system, as well as making it more efficient. For example, the calculated convective heat transfer coefficient (HTC) is shown in Figure 40. For illustration purposes, the HTC is shown for the region near the cooler. Defining the Nusselt number (Nu),

$$Nu = \frac{hx}{k} \tag{5}$$

h= convective heat transfer coefficient (HTC)

X=characteristic length (pipe diameter)

K=fluid thermal conductivity

Nu can therefore be calculated from the CFD calculation, the pipe diameter, and the fluid thermal conductivity; its magnitude is shown in Figure 38. It is noted here that the fluid properties were calculated by RELAP5 as volume-cell averages; ideally, the film temperature could be used, as many heat transfer

correlations were developed using film temperature properties. Note also that the characteristic length was chosen as the pipe diameter D for this system; for flat plates, the plate height is the characteristic dimension. Figure 38 shows laminar (dash blue line with open circles) and turbulent (dash-dot red line with closed circles) correlations for natural circulation, respectively. The figure shows the desirable impact of turbulence, as a higher Nu will result in higher convective heat transfer. The calculations showed that the SCO_2 fluid quickly became turbulent, which is clearly a desirable design feature for this system. Additional natural circulation turbulence and therefore enhanced heat transfer can be attained by using mixing plates and swirl vanes [18, 19].

The laminar Nu was calculated from [20, 21], as follows,

$$Nu_{lam} = 0.6\ (GrPr)^{0.25} \tag{6}$$

The turbulent Nu was computed as the average of two correlations [20],

$$Nu_{turb} = 0.021\ (GrPr)^{2/5} \tag{7a}$$

$$Nu_{turb} = 0.1\ (GrPr)^{1/3} \tag{7b}$$

Where

$$Gr = Grashof\ number = \frac{\beta g \Delta T x^3}{\nu^2} \tag{8}$$

ν =μ/ρ=fluid kinematic viscosity

ρ=fluid density

μ=fluid dynamic viscosity

g=gravitational constant

ΔT= wall fluid temperature gradient

X=pipe diameter=D

$$Pr = \frac{C_p \mu}{k} \tag{9}$$

C_p= heat capacity at constant pressure

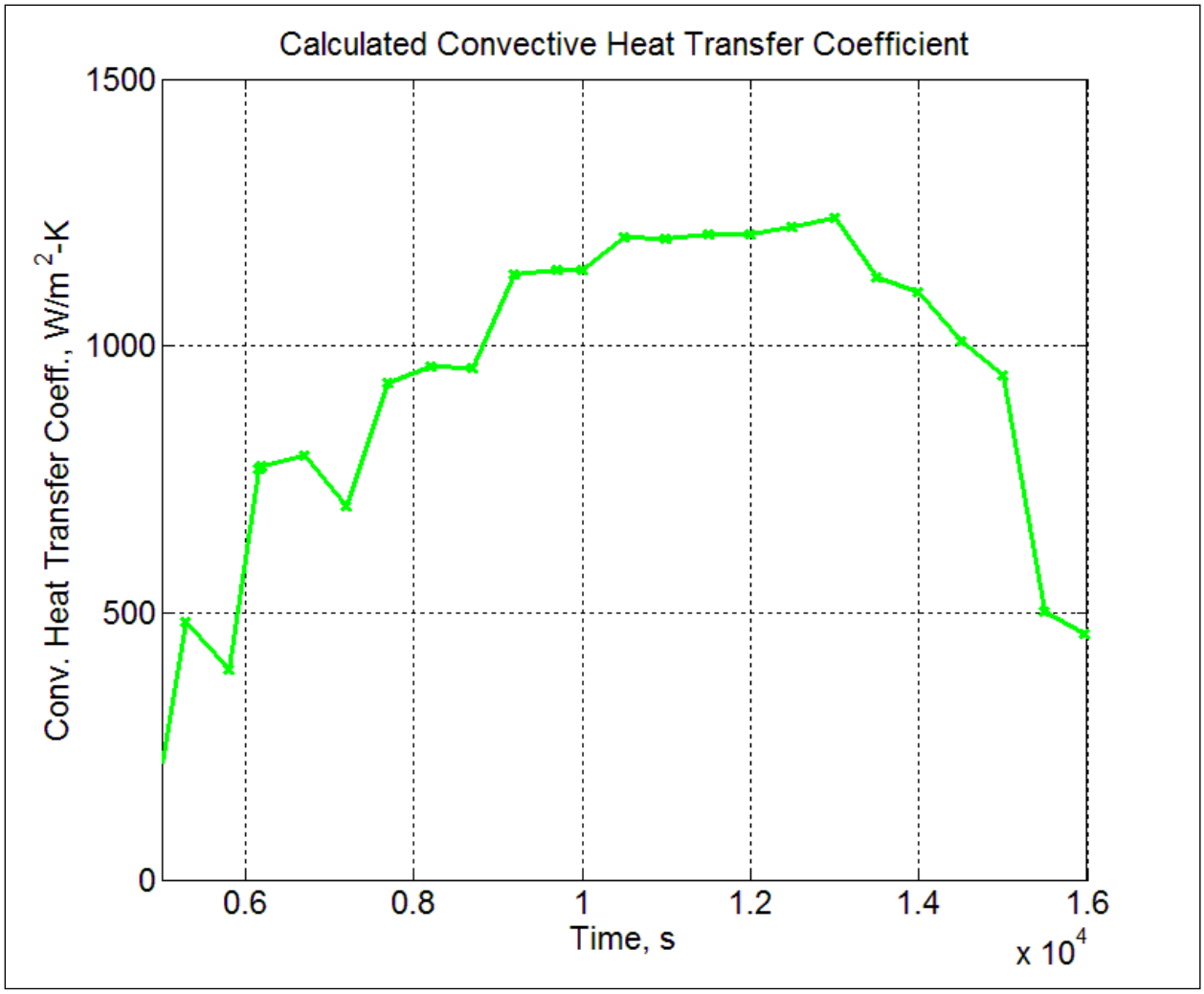

Figure 38 Convective Heat Transfer Coefficient.

The Grashof number (Gr) and Prandtl number (Pr) can be obtained from the calculated properties, and are shown in Figure 39 and 43, respectively. Both Gr and Pr form the basis for natural circulation heat transfer. In fact, they are directly derivable from momentum and energy conservation [20].

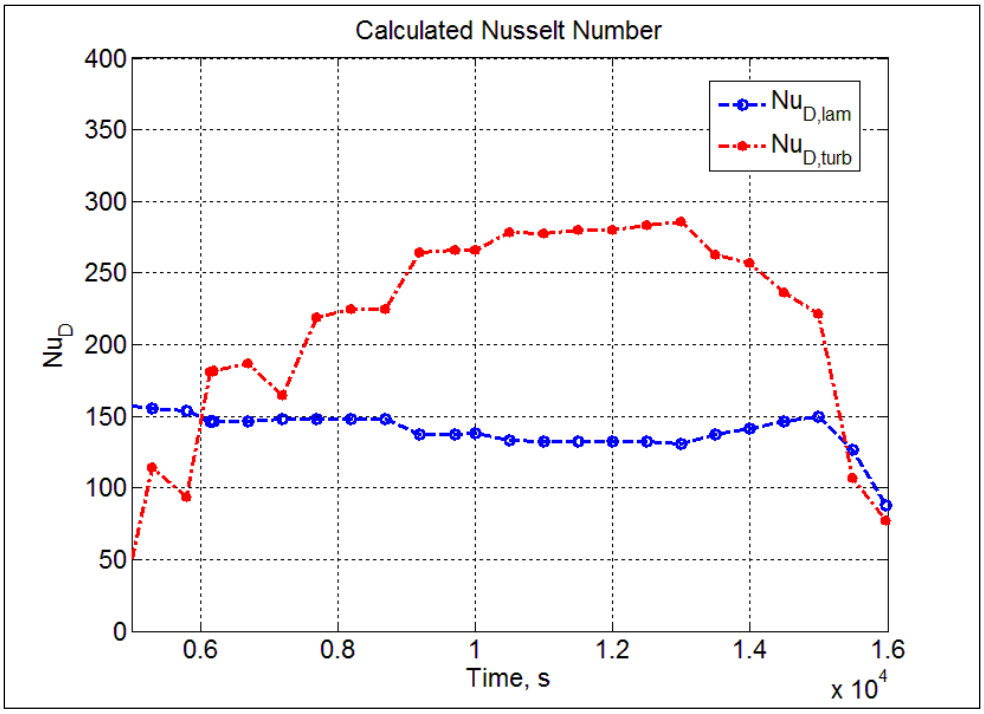

Figure 39 Nu vs. time.

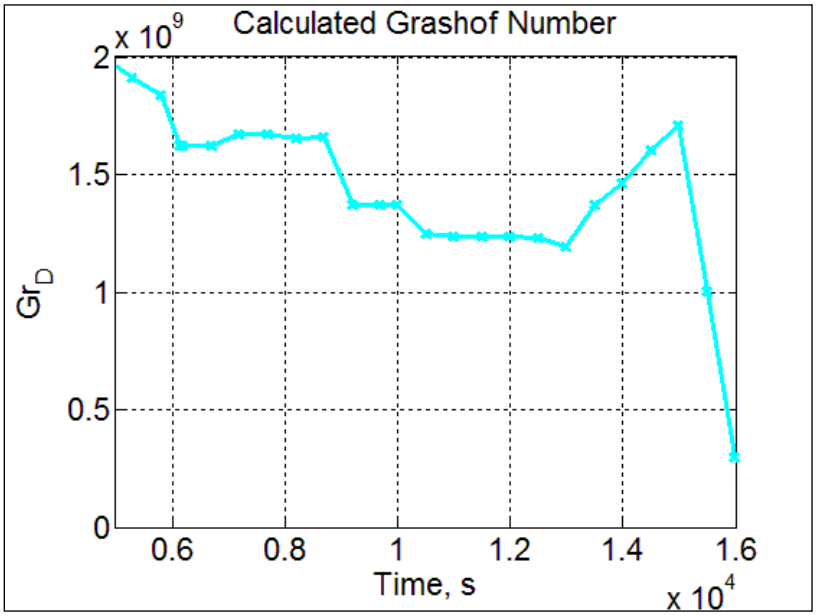

Figure 40 Gr vs. time.

Finally, the product of Gr and Pr is used to obtain the Rayleigh number, which provides an indication of fluid laminarity or turbulence,

$$Ra=GrPr \tag{10}$$

Ra is shown in Figure 42. For a vertical plate, GrPr < 10^9 implies laminar natural circulation; GrPr > 10^9 implies turbulent natural circulation [20]. Thus, the fluid is fully turbulent, except near the experiment-initiation time and near its termination point. Therefore, with regards to scaling, it must be conducted such that the fluid boundary layer grows non-linearly in a turbulent, parabolic distribution. Further, once the piping is full of boundary layer, additional loop height will not result in additional heat transfer. Thus, the system is clearly optimizable and can be scaled appropriately under these constraints.

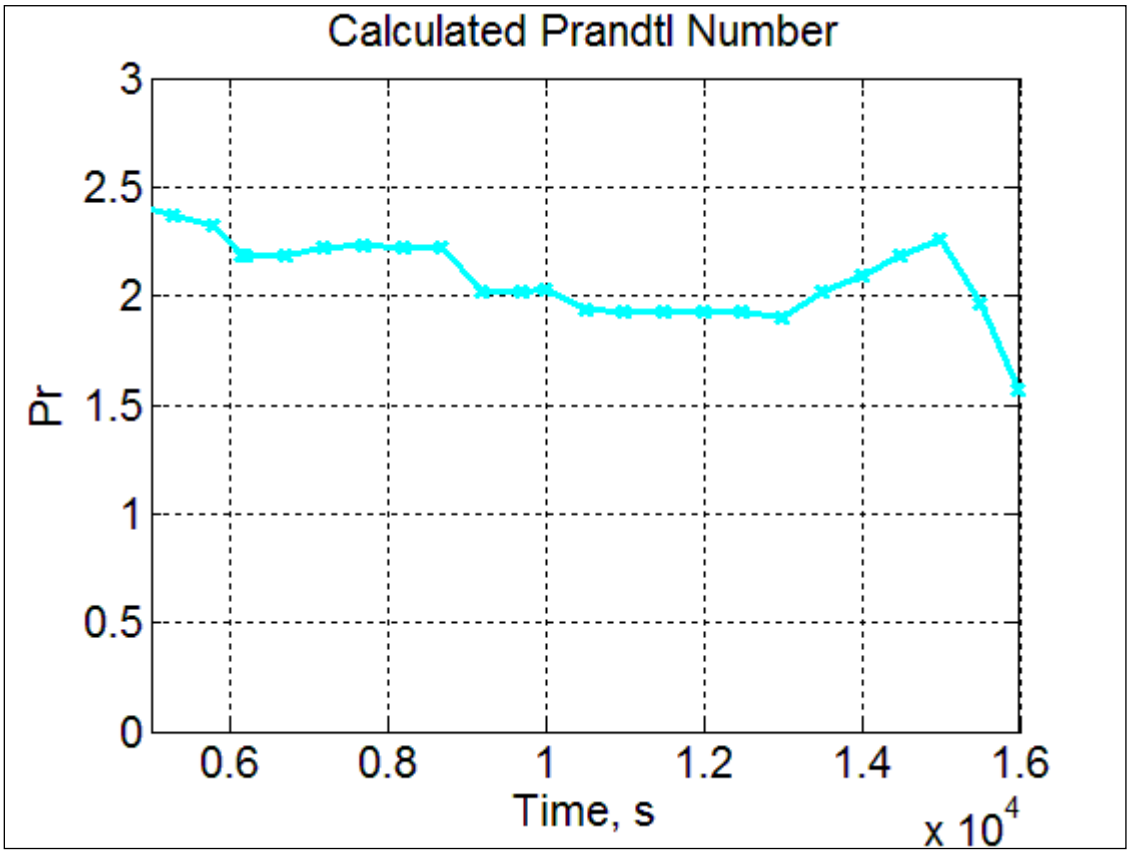

Figure 41 Pr vs. time.

By using Equations 5, 7B, 8, and 9,

$$Nu_{turb} = \frac{hx}{k} = 0.1\,(GrPr)^{1/3} = \left(\frac{\beta g \Delta T x^3}{\nu^2}\frac{C_p \mu}{k}\right)^{1/3} = \left(\frac{\beta g \Delta T}{\nu^2}\frac{C_p \mu}{k}\right)^{1/3} \text{x} \tag{11a}$$

$$h_{turb} = \left(\frac{\beta g C_p \rho^2 k^2 \Delta T}{\mu}\right)^{1/3} \neq h_{turb}(\text{x}) \tag{11b}$$

Therefore, for fully-turbulent natural circulation, HTC is not a function of x, and scaling about x is therefore trivial. The same type of argument can be made for ΔT, but with the following conclusion.

$$h_{turb} \approx \Delta T^{1/3} \tag{12}$$

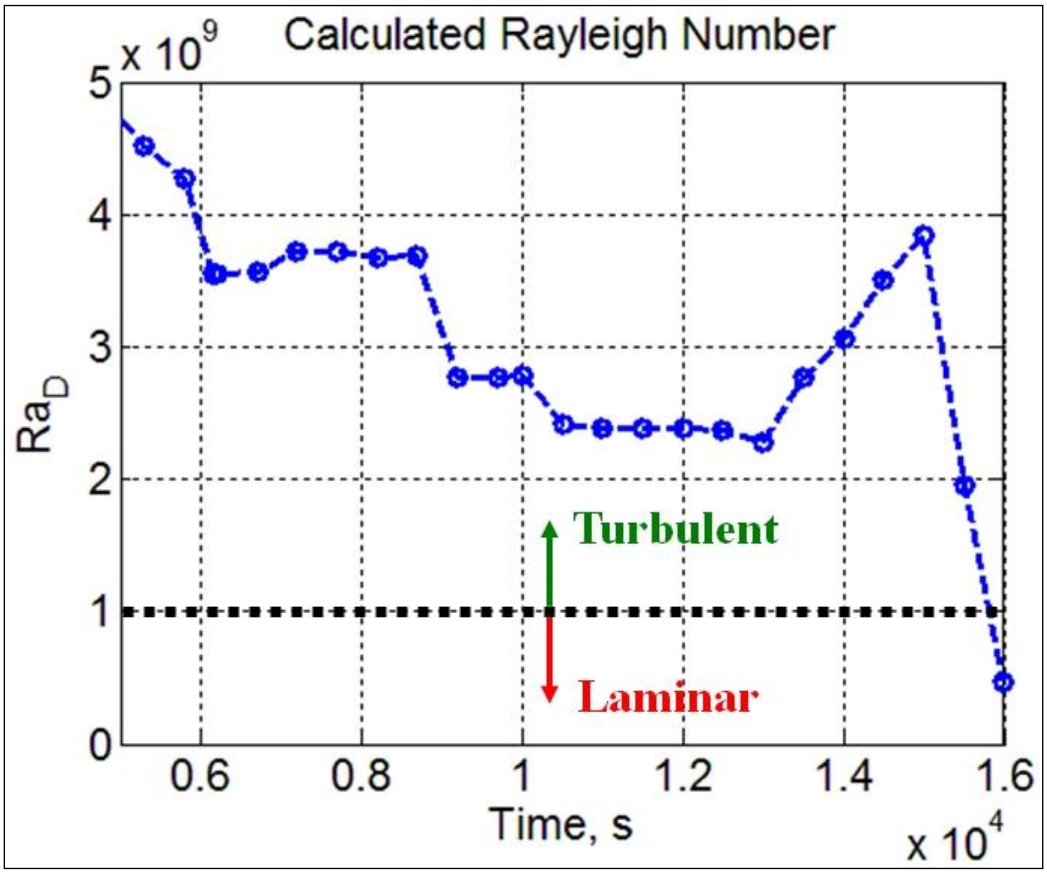

Figure 42 Ra vs. time.

5 Conclusions

5.1 Conclusions from LDRD Project

This LDRD project demonstrated that sCO_2 can be utilized for purposes that benefit from natural circulation potential and from dry heat rejection. Repeated operation of an air-cooled, naturally circulating sCO_2 loop in a laboratory environment showed that, at least on the laboratory scale, sCO_2 can be utilized to transfer heat from one source to the surrounding air with not significant control problems.

For the purpose of utilizing sCO_2 as the working fluid in a decay heat removal system for nuclear power, no obvious barriers were observed. The sCO_2 was easily controlled from a stationary starting state, especially when the heated section was on a vertical portion of the loop.

Modeling of the loop was successful, even without knowing the specifics of the air cooler. The interior design of the Xchanger air cooler was not available to be studied. However, the Relap5 and CFD model reproduced the laboratory observations to within 10% for transient observations. The FUEGO model also showed that the 3-dimensional effects of the flow can be modeled.

Utilizing the models and the data, dimensionless parameters could be estimated and show that scaling predictions can be made. This is very important for the next phase of work that needs to be completed.

5.2 Future Considerations

This project laid the groundwork for the use of sCO_2 in natural circulation and dry heat rejection scenarios. However, much work needs to be completed to enable this to be used in real-world situations. Some projects that should be investigated include the following.

- Scaling analysis for real-world sizing – The ability to develop accurate CFD models shows that natural circulation of sCO_2 does not have any anomalous characteristics that would prevent it from being used in situations that can benefit from natural circulation. However, the tubing used in this LDRD project was 1” OD tubing with a wall thickness of 0.095”. Thus the interior diameter of the tube was only 0.81”. The maximum heating rate achieved thus far is on the order of 15 kWth. To be utilized in the decay heat removal system for a 300 MWe SMR, the system would need to be able to reliably transfer at least 70 MW of thermal energy to the atmosphere. Thus, scaling analysis needs to be completed so that a more appropriately-sized demonstration loop can be developed in the future. 3-D effects, such as convective currents in the loop, will become more prominent in larger systems.
- Assessment of dry-heat rejection technology – Although this experiment demonstrated that dry air can be used to cool the sCO_2, the cooler being used was a forced-air cooler. This is possible in aSMR systems; however, the design of a natural draft air cooler for such a decay heat removal system would be ideal to ensure that the decay heat is removed in the event of Station Blackout (SBO). This work may include materials research to determine the long-term effects of sCO_2 on the materials as well as to determine the heat transfer coefficients for heat exchangers. A first step in this work would be to perform a gap analysis on sCO_2-to-air heat exchanger technology.

- Optimal control around the critical point and pseudocritical points – As can be seen in Figure 20, the state of a supercritical fluid moves further away from the point of maximum specific heat capacity as the fluid is heated. Thus, a decay heat removal system will gain the largest change in density between the hot and cold legs when heat is added very near the critical point. However, a heat sink could possibly gain some advantage by maintaining a state point near the pseudocritical points because this minimized the temperature rise in the fluid for a given heat input. A control strategy that could automate such a system may find uses in safety systems.

References

[1] U.S. Energy Information Administration, *July 2015 Monthly Energy Review*, http://www.eia.gov/totalenergy/data/monthly/pdf/mer.pdf, DOE/EIA-0035(2015/07), U.S. Energy Information Administration, July 28 2015.

[2] World Nuclear Association, *Nuclear Power in the USA*, http://www.world-nuclear.org/info/Country-Profiles/Countries-T-Z/USA--Nuclear-Power/, August 11 2015.

[3] LaChance, Jeffrey, Gregory Baum, Felicia Duran, Kathy Ottinger Farnum, Sabina Jordan, Bobby Middleton, and Timothy Wheeler, *Evaluation of the Applicability of Existing Nuclear power Plant Regulatory Requirements in the U.S. to Advanced Small Modular Reactors,* SAND2013-3683, Sandia National Laboratories, Albuquerque, NM, May 2013.

[4] (OUO) Conboy, Thomas M., James Pasch, Darryn Fleming, and Gary E. Rochau, *High Temperature Re-Compression Brayton Cycle Design Completion, Delivery, and Commissioning,* SAND2015-1773, Sandia National Laboratories, Albuquerque, NM, October 2012.

[5] REFPROP, Reference Fluid Thermodynamic and Transport Properties, Database 23, Version 9.1, www.nist.gov/srd/upload/REFPROP9.PDF.

[6] Bauer, Diana, "Water-Energy Nexus: Challenges and Opportunities," US Department of Energy, Office of Energy Policy and Systems Analysis, Water-Energy Tech Team (WETT), September 5, 2014.

[7] Mays, G.T., R.J. Belles, B.R. Blevins, S.W. Hadley, T.J. Harrison, W.C. Jochem, B.S. Neish, O.A. Omitaomu, and A.N. Rose, "Application of Spatial Data Modeling and Geographical Information Systems (GIS) for Identification of Potential Siting Options for Various Electrical Generation Sources," ORNL/TM-2011/157, December 2011.

[8] McKinnon, Shaun, "5 Cities Cash in on Wastewater Deal with Palo Verde," *Arizona Business & Money*, http://archive.azcentral.com/business/articles/2010/04/01/20100401water-paloverde0401.html, April 1, 2010.

[9] Wald, Matthew L., "Oyster Creek Reactor to Close by 2019," *The New York Times,* December 8 2010.

[10] Middleton, Bobby D., "Sandia National Laboratories' Air-Cooled Natural Circulation Loop for Supercritical Carbon Dioxide," Presented at ASME 2015 Power Energy Conference, San Diego, CA, July1 2015.

[11] Conboy, Thomas, "S-CO_2 as an Enabling Technology for Dry-Cooled Nuclear Power," Presented at ASME 2014 Small Modular Reactors Symposium, Washington, DC, April 15, 2014.

[12] Tsou, John L., John Maulbetsch, and Jessica Shi, "Power Plant Cooling System Overview for Researchers and Technology Developers", EPRI Report 3002001915, May, 2013.

[13] Delgado, Anna and Howard J. Herzog, "A Simple Model to Help Understand Water Use at Power Plants," Massachusetts Institute of Technology, Energy Initiative.

[14] Doda, N. et al, "Development of Core Hot Spot Evaluation Method for Natural Circulation Decay Heat Removal in Sodium Cooled Fast Reactor," *Proceedings of the 14th International Topical Meeting on Nuclear Reactor Thermal Hydraulics (NURETH-14),* Toronto, Canada, 2011, NURETH14-170, 13p.

[15] RELAP5, RELAP5-3D/4.0, Volume II Appendices, INEEL-EXT-98-00834-V2, 1998.

[16] Fuego, "SIERRA/Fuego 2.7 User's Manual", Sandia National Laboratories, SAND 2006-6084P, 2008.

[17] RPL (Rocket Propulsion Laboratory), "Aerospace Fluid Component Designer's Handbook", Sections 1-6, 1970.

[18] Rodriguez, S., "Swirling Jets for the Mitigation of Hot Spots and Thermal Stratification in the VHTR Lower Plenum", PhD diss., University of New Mexico, 2011.

[19] Rodriguez, S., "Turbulence II: Natural Circulation Class Notes, Fall 2014", University of New Mexico, 2014.

[20] Holman, J., *Heat Transfer,* 7th Edition, McGraw-Hill, Inc., 1990.

[21] Rodriguez, S. and D. Ames, "Design Optimization of Miniature Nuclear Reactors", American Nuclear Society Winter Meeting, 2015.

6 Distribution

1	MS0721	Susan Pickering	6200
1	MS0736	Evaristo Bonano	6220
1	MS1136	Gary Rochau	6221 (electronic copy)
1	MS1136	Bobby Middleton	6221 (electronic copy)
1	MS1136	Sal Rodriguez	6221 (electronic copy)
1	MS1136	Matt Carlson	6221 (electronic copy)
1	MS0899	Technical Library	9536 (electronic copy)
1	MS0359	D. Chavez, LDRD Office	1911


Sandia National Laboratories